JGR Solid Earth

RESEARCH ARTICLE
10.1029/2021JB023328

Bilateral Heterogeneity in an Upwelling Mantle via Double Subduction of Oceanic Lithosphere

Nghiem Van Dao[1,2], Hiroshi Kitagawa[1], Eizo Nakamura[1], Katsura Kobayashi[1], Thanh Xuan Ngo[2], and Son Hai Trinh[3]

[1]The Pheasant Memorial Laboratory for Geochemistry and Cosmochemistry, Institute for Planetary Materials, Okayama University, Misasa, Japan, [2]Department of Geology, Hanoi University of Mining and Geology, Hanoi, Vietnam, [3]Vietnam Institute of Geoscience and Mineral resources, Hanoi, Vietnam

Key Points:

- New isotopic data of Vietnamese basalts reveals that they exist within isotopically distinct subpopulations in Central and Southern Vietnam
- Basalts in Central and Southern Vietnam with distinct isotopic signatures are of sub-lithospheric origin, suggested by melting conditions
- Vietnamese basalts were extracted from different mantle domains, separated by convection induced by the Pacific and Indo-Australian plates

Supporting Information:

Supporting Information may be found in the online version of this article.

Correspondence to:

H. Kitagawa,
kitaga-h@okayama-u.ac.jp

Citation:

Dao, N. V., Kitagawa, H., Nakamura, E., Kobayashi, K., Ngo, T. X., & Trinh, S. H. (2022). Bilateral heterogeneity in an upwelling mantle via double subduction of oceanic lithosphere. *Journal of Geophysical Research: Solid Earth*, *127*, e2021JB023328. https://doi.org/10.1029/2021JB023328

Received 28 SEP 2021
Accepted 9 MAY 2022

Abstract Vietnam is a major field of Cenozoic volcanism in Southeast (SE) Asia. Two contrasting models have been proposed to explain the mantle upwelling and volcanism in this region; collision of the Indian and Eurasian continents or subduction of the Pacific or Indo-Australian oceanic lithosphere. To place constraints on the origin of the intraplate volcanism in SE Asia, new geochronological and geochemical data for Cenozoic basalts in Vietnam are presented. Based largely on Sr-Nd-Pb isotope systematics, it was found that the sources of basalts from Central and Southern Vietnam are chemically distinct forming a sharp boundary at 13.5°N. The basalts north of the boundary show isotopic features similar to Enriched Mantle type 2 (EM2) ocean island basalts. Whereas the basalts south of the boundary show isotopic features similar to Enriched Mantle type 1 (EM1) ocean island basalts. The EM1 and EM2 basalts display positive Sr anomalies and elevated Pb/Ce and Th/La ratios, respectively. Such features suggest the origins of the sources through the recycling of deeply-subducted crustal lithologies. Furthermore, subduction of dense oceanic lithosphere can induce a convecting cell in the upper mantle. Therefore, we suggest that the chemically different basalts from Central and Southern Vietnam represent the surface expression of melting in two different convecting cells, one is driven by subduction of the Pacific plate and the other by subduction of the Indo-Australian plate.

Plain Language Summary Many of Earth's volcanoes are associated with the margins of tectonic plates, where plates are diverging from or converging with each other. However, some volcanoes occur in areas away from the plate margins and are termed intraplate volcanoes. Active upwelling in the mantle is a primary cause of intraplate volcanism, which is considered to arise due to several factors (e.g., heat or water sources in the deep mantle). Here we conducted a geochemical investigation of the volcanic rocks from Vietnam in Southeast Asia. We found that the volcanic-rock series in Central and Southern Vietnam have different chemical compositions. The result indicates that two distinct mantle domains exist beneath Vietnam, and these domains contain materials inherited from the plates that were subducted deep beneath Vietnam. We conclude that plate subduction could induce volcanic activity not only in areas close to plate margins but also in areas far from them.

1. Introduction

Intraplate-basaltic volcanism was widespread throughout Southeast (SE) Asia during the Cenozoic (Figure 1; Flower et al., 1998). Vietnam is located at the southeastern edge of SE Asia (Figure 1a) and represents the most volcanically active field on the Indochina Peninsula (Figure 1b; Flower et al., 1998). The upwelling of hot asthenospheric materials, revealed by seismic tomography (Huang et al., 2015), is considered to be a primary cause of the volcanism in this region.

Lithospheric thinning, induced by the collision of the Indo-Australian plate and Eurasian plate, has long been proposed as a cause of asthenospheric upwelling (Flower et al., 1998; Hoang et al., 1996; Hoang & Flower, 1998). In this model, the asthenospheric upwelling is confined to the uppermost mantle, and the isotopic variability of Vietnamese basalts is due to the various extents of interaction between asthenosphere-derived melts and the overlying lithosphere (Hoang et al., 1996; Hoang & Flower, 1998). Instead, recent studies argued that asthenospheric upwelling was derived from deeper regions, for example, the core-mantle boundary (An et al., 2017; Hoang et al., 2018; Wang et al., 2013; Yan et al., 2018). This model ascribes the isotopic variability of Vietnamese basalts to the intrinsic heterogeneity of the asthenosphere (An et al., 2017). Hoang et al. (2018) argued

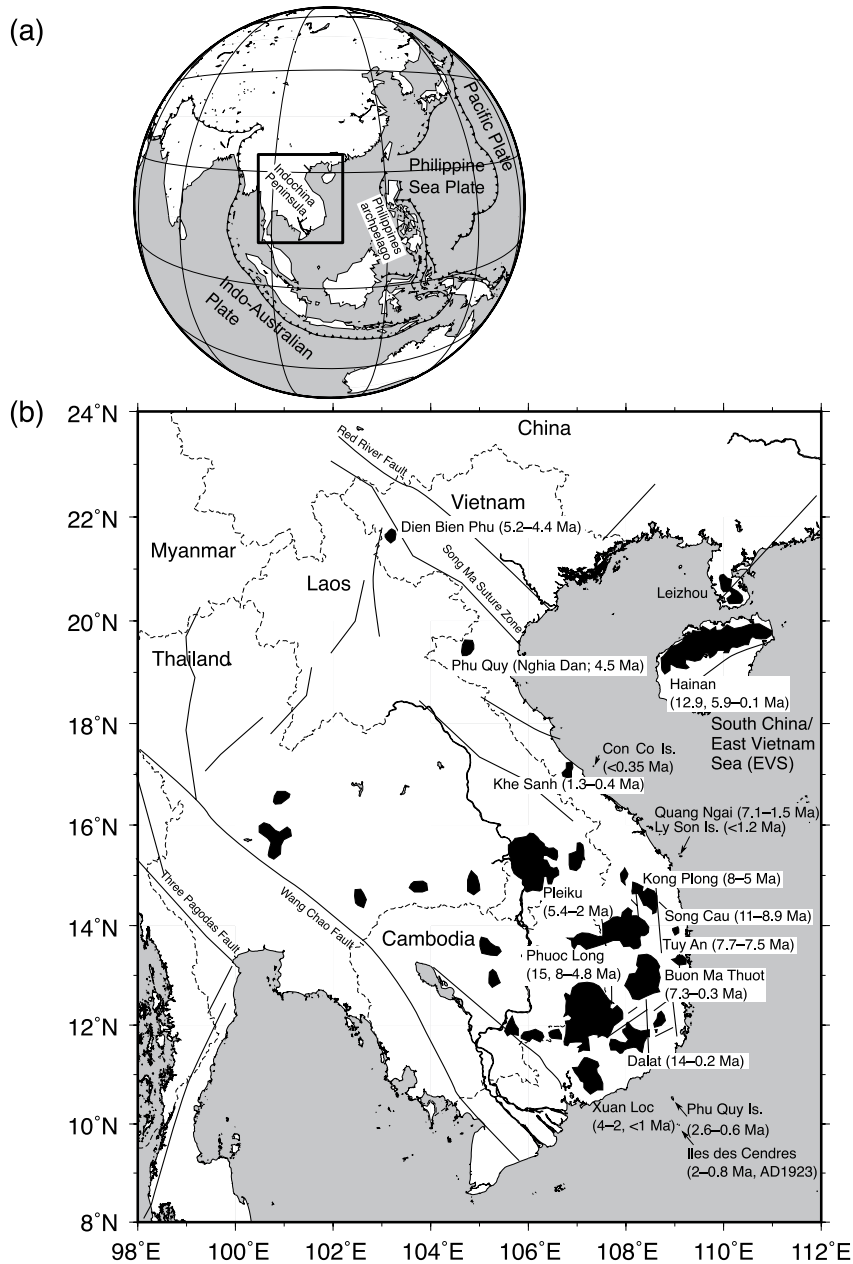

Figure 1. (a) Plate configuration in east Asia. (b) Map of Indochina Peninsula showing distribution of Cenozoic mafic volcanic rocks. Ages of volcanic rocks (by K-Ar and $^{40}Ar/^{39}Ar$ methods) from each volcanic field are shown in parenthesis (data source: this study; An et al., 2017; Barr & Macdonald, 1981; Ho et al., 2000; Le et al., 2019; Lee et al., 1998; Rangin et al., 1995; Sieh et al., 2020; Wang et al., 2012).

that asthenospheric upwelling is centered on Hainan Island (seismically detected as the Hainan plume; Montelli et al. [2006]), and thus the geochemistry of Vietnamese basalts shows lateral variation with distance from the island. However, the effect of the Hainan plume remains elusive, for example, estimates of the mantle potential temperature for the production of basaltic magmas in Vietnam (T_p = 1470–1490°C; An et al. [2017]) are lower by 50°C or more than that estimated for Hainan basalts (1540°C; Wang et al., 2012). Instead, the estimated temperatures for Vietnam are rather similar to recent estimates of T_p for ambient upper mantle (1400–1460°C; Putirka [2016]; Sarafian et al. [2017]).

As an alternative to the two conventional models outlined above, another model deduced from numerical experiments was proposed to explain the intraplate volcanism (Dasgupta & Mandal, 2022; Lyu et al., 2019). The models

explain how dense oceanic lithosphere, subducted to the mantle transition zone (MTZ), can induce asthenospheric upwelling from the MTZ without elevating temperature. In the other areas adjacent to SE Asia, intraplate basaltic volcanism had occurred contemporaneously, including in Northeast Asia, and Eastern Australia and Zealandia. Petrologic and geochemical characteristics of these basalts show evidence that is consistent with this scenario (e.g., Kuritani et al., 2011; Mather et al., 2020; Nakamura et al., 1986, 1985; Sakuyama et al., 2013). Given that the recent seismic data detected stagnant slabs that are widely distributed within the SE Asian mantle (Huang et al., 2015; Yu, Gao, et al., 2017), these examples may be analogous to intraplate volcanism in the Indochina Peninsula. Therefore, it is important to assess this model further.

In this study, the K-Ar ages, major- and trace-element abundances, and Sr-Nd-Pb isotopic compositions of Cenozoic basalts are investigated across all of Vietnam. These data are combined with published geochemical data and used to address the possible scenarios and elaborate a new model for the origin of Vietnamese volcanism.

2. Geological Settings and Samples

Southeast Asia is surrounded by convergent plate margins (Figure 1a). The Indo-Australian plate is subducting in the southwest of SE Asia and the Philippine Sea plate is subducting in the east of SE Asia. The leading edge of the Indo-Australian plate reaches the MTZ beneath the southern part of the Indochina Peninsula (Huang et al., 2015; Pesicek et al., 2008; Yu, Gao, et al., 2017). The Philippine Sea plate is shallowly subducting (100–400 km) beneath the Philippines archipelago (Fan & Zhao, 2019; Wu et al., 2016). More than 4000-km to the east, the Pacific plate is subducting beneath the Philippine Sea plate, and its leading edge reaches the MTZ beneath the northern Indochina Peninsula (Fukao & Obayashi, 2013; Yu, Gao, et al., 2017; Zhao et al., 2021).

The basement terranes of the Indochina Peninsula are mainly comprised of a continental block (Indochina block) bordered by strike-slip faults or suture zones (Figure 1b). The Indochina block is a fragment of Gondwanaland and was extruded from the northwest by the collision of the Indo-Australian plate and Eurasian plate during 55–50 million years ago or Ma (Hall, 2002; Metcalfe, 2013). The upper crust of the block is dominantly composed of Proterozoic felsic rocks (granulites, gneisses, and granites; Lan et al. [2003]). In Southern Vietnam, the upper crust, capped by Cenozoic basalts, also contains Cretaceous granitic rocks (Nguyen, Satir, Siebel, Vennemann, & Van Long, 2004; Nguyen, Satir, Siebel & Chen, 2004). A receiver function analysis suggests that the crust beneath Central Vietnam has an overall felsic composition, whereas that beneath Southern Vietnam has a layered structure of felsic and mafic compositions in the upper and lower parts, respectively (Yu, Hung, et al., 2017). Details about the basement geology and lithology are given in Text S1 in Supporting Information S1.

Following the continental collision, the oceanic lithosphere of the Indo-Australian plate began to subduct and led to the spreading of a marginal sea basin, the East Vietnam Sea/South China Sea (EVS/SCS) at *c*. 30 Ma (Clift et al., 2008). Subsequently, basaltic volcanism began in subaerial regions of the Indochina Peninsula and adjacent regions, including Hainan, Laos, Thailand, Cambodia, and Vietnam (Figure 1b; Barr & Macdonald, 1981; M. F. J. Flower et al., 1992, Flower et al., 1998; Y.-Q. Li et al., 2020; Sieh et al., 2020; Wang et al., 2012; Yan et al., 2018; Zhou & Mukasa, 1997). Seamounts in the EVS/SCS, dated at 11–0.4 Ma, are also products of concurrent volcanic activity (Kudrass et al., 1986; Tu et al., 1992; Yan et al., 2008).

Vietnam has been the most volcanically active field of the Indochina Peninsula, having produced lava plateaus with an aerial extent of 23,000 km^2 (Hoang et al., 1996, 2013; Hoang & Flower, 1998). Thirteen volcanic fields are recognized in Vietnam (Figure 1b; Lee et al. [1998]); Dien Bien Phu, Phu Quy (or Nghia Dan), Khe Sanh, Con Co Island, Quang Ngai, and Ly Son Island (or Re Island), Kong Plong, Pleiku, Song Cau, Buon Ma Thuot, Phuoc Long, Dalat, Xuan Loc, and Phu Quy Island and Ile des Cendres from north to south. Of the 13 volcanic fields, 8 were surveyed and 70 mafic volcanic rocks were collected (Figure 1 and Figure S1 in Supporting Information S1).

The EVS/SCS was also volcanically active during the Cenozoic. Eruptions of basalts occurred during *c*. 30 to 16 Ma in axial zones and *c*. 20 to 0.5 Ma in off-axis zones (C.-F. Li et al., 2014; Tu et al., 1992; Yan et al., 2008, 2015; Zhang, Luo, et al., 2018, 2018b). The major- and trace-element abundances and Sr-Nd isotope compositions of basalts collected by the International Ocean Discovery Program (IODP) Expedition 349 from the site U1431 ($n = 7$) and the site U1433 ($n = 3$), were analyzed. The basalts represent magmas erupted at spreading centers at different locations and periods.

3. Analytical Methods

Major- and trace-element and Sr-Nd-Pb isotope analyses and K-Ar dating were performed at the Pheasant Memorial Laboratory, Institute for Planetary Materials, Okayama University at Misasa (Nakamura et al., 2003). Whole-rock samples were crushed by a jaw crusher into fragments, and those of 5–10 mm size were hand-picked. To avoid the artificial loss or gain of specific phenocryst phases, fragments <5 mm were excluded. Visible xenoliths and xenocrysts were also removed. Selected fragments were cleaned by ultrasonication in de-ionized water, and dried in an oven at 110°C overnight. Dried fragments were then pulverized using an alumina ceramic puck mill. Major-element concentrations and Ni and Cr contents were determined by X-ray fluorescence spectrometry (XRF) with a Philips PW2400 instrument, using lithium tetraborate glass beads (1:10 ratio of sample and flux) as outlined in T. T. Nguyen et al. (2020). Loss on ignition (LOI) was obtained by the gravimetric method; samples were heated at 1000°C in a furnace (>4 hr), and weight loss or gain values were measured using a balance. Trace-element concentrations were determined by inductively coupled plasma mass spectrometry (ICPMS) with instruments Agilent 7500cs and Thermo Scientific iCAP TQ instruments. The procedures of sample decomposition and the determination of elemental abundances follow Yokoyama et al. (1999), Tanaka et al. (2003), Makishima and Nakamura (2006), and Lu et al. (2007). All analyses were duplicated, and the relative difference between them are better than 1% for major elements and 3% for trace elements [except for B (<5%, ICPMS), Be (<9%, ICPMS), Cr (<5%, XRF), Ni (<5%, XRF), Cs (<6%, ICPMS) and Ta (<5%, ICPMS)], respectively.

Strontium, Nd, and Pb isotopic compositions were analyzed by a thermal ionization mass spectrometry in a static multi-collection mode (with Thermo Scientific TRITON and TRITON Plus instruments). Separation procedures for Sr, Nd, and Pb follow Yoshikawa and Nakamura (1993), Nakamura et al. (2003), and Kuritani and Nakamura (2002), respectively. Samples for isotopic analyses were leached in 6 M HCl (100°C, 6 hr) to minimize the effect of contamination. Instrumental mass bias was internally corrected for Sr and Nd, using $^{86}Sr/^{88}Sr = 0.1194$ and $^{146}Nd/^{144}Nd = 0.7219$, respectively. The $^{87}Sr/^{86}Sr$ and $^{143}Nd/^{144}Nd$ ratios of samples are reported relative to NIST SRM 987 $^{87}Sr/^{86}Sr = 0.710250$ and La Jolla $^{143}Nd/^{144}Nd = 0.511860$, respectively. Instrumental mass bias during Pb isotope analysis was corrected by the double-spike method (Kuritani & Nakamura, 2003). The NIST SRM 981, analyzed during this study, yields $^{206}Pb/^{204}Pb = 16.9422 \pm 0.0017$, $^{207}Pb/^{204}Pb = 15.4997 \pm 0.0019$, and $^{208}Pb/^{204}Pb = 36.7270 \pm 0.0043$ (2σ, $n = 24$). The compiled Sr, Nd, and Pb isotope data are also normalized relative to these reference materials. The external reproducibilities (2σ) of Sr, Nd, and Pb isotope analyses are 30, 50, and 100 ppm, respectively, based on repeated analyses of the reference standard materials (JB-2 for Sr and Nd, and JB-3 for Pb, see Table S1).

The K-Ar ages were obtained by analyses of Ar abundance by a noble gas mass spectrometer (Micromass VG5400) and K abundance by a flame photometer (Shimadzu AA-6200) following T. T. Nguyen et al. (2020). Groundmass fractions were used for both K and Ar analyses. Instrumental mass bias during Ar isotopic analysis was externally corrected using reference air. All analyses were duplicated. Details of analytical procedures can be found in Text S2 in Supporting Information S1.

4. Results

Results of geochronological and geochemical analyses are summarized in the Supporting Information (Tables S1–S4 in Supporting Information S1), which includes K-Ar ages ($n = 19$), major-element abundances ($n = 70$), trace-element abundances ($n = 49$), and Sr-Nd-Pb isotopic compositions ($n = 38$) for subaerial samples. Additionally, major- and trace-element abundances, and Sr-Nd isotopic compositions of the seafloor basalts from the EVS/SCS ($n = 10$) are also reported.

4.1. Petrography

Mafic volcanic rocks in the studied area are classified into either alkaline or sub-alkaline series based on whole-rock major-element compositions and normative mineral compositions (Figure 2a and Table S2 in Supporting Information S1). Irrespective of rock series, most rocks show aphyric to sparsely-phyric textures with <10 vol% phenocrysts consisting of olivine (<10 vol%), clinopyroxene (<5 vol%), and plagioclase (<15 vol%) (Figure S2 in Supporting Information S1). Alkaline rocks have less abundances of plagioclase phenocrysts (<5 vol%) than sub-alkaline rocks in the same volcanic field. Sub-alkaline rocks are generally phyric (2–10 vol% phenocryst),

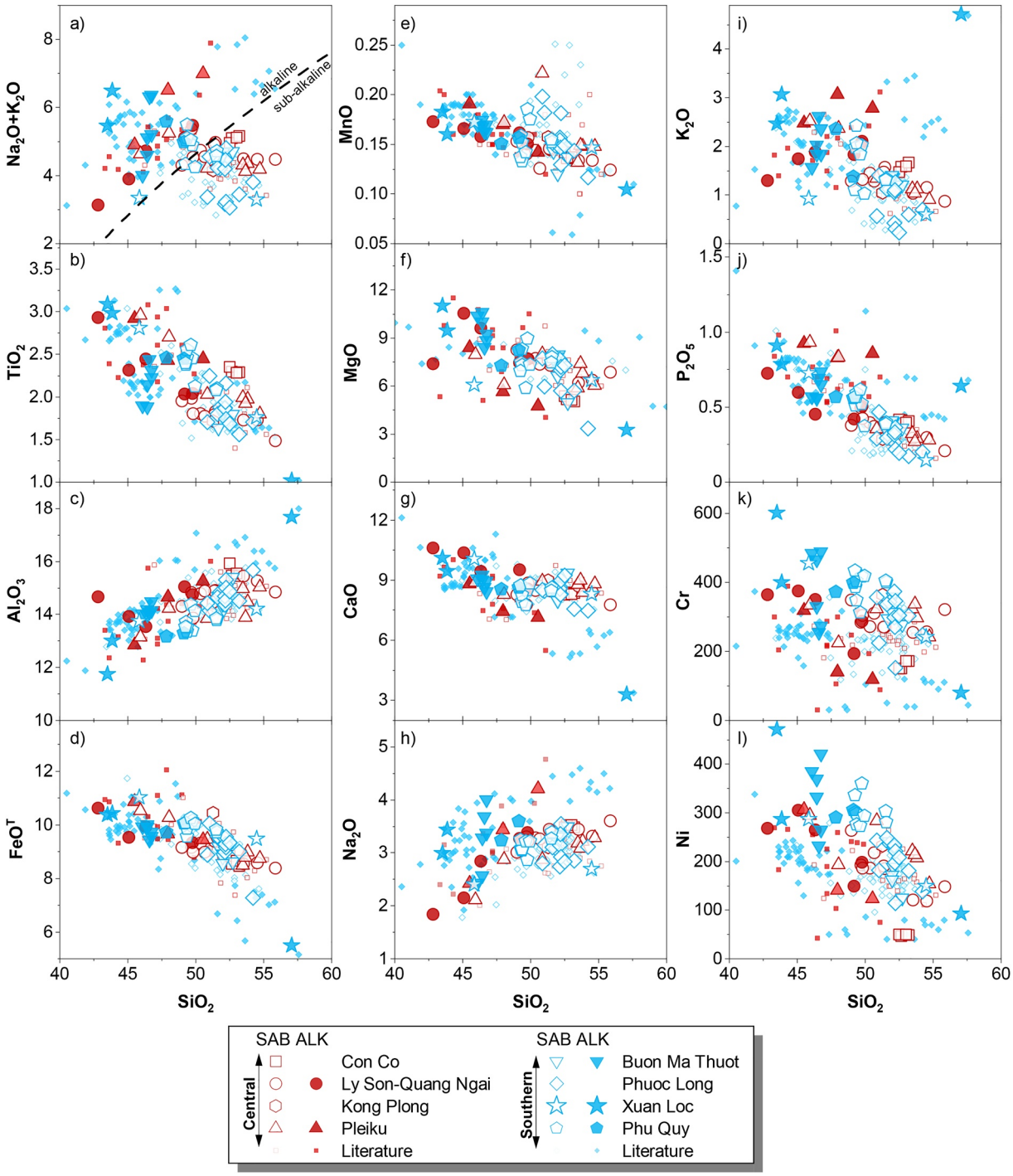

Figure 2. Major-element (in wt%) and Cr Ni (in ppm) concentrations plotted against SiO_2 (in wt%). The dashed line in (a) divides samples into the alkaline and sub-alkaline series (Irvine & Baragar, 1971). Open and filled symbols indicate sub-alkaline (SAB) and alkaline series (ALK), respectively, which are classified by normative mineral compositions (CIPW, Table S2). Literature data are from An et al. (2017), Hoàng et al. (2013), Hoang et al. (1996, 2019), and Hoang et al. (2018).

and those from Phuoc Long and Xuan Loc are porphyritic with 10–15 vol% plagioclase. Detailed petrographic descriptions for each volcanic field are provided in Supporting Information S1 (Text S3 and Figure S2 in Supporting Information S1).

4.2. K-Ar Ages

Previous studies reported ages as old as 15 Ma for mafic volcanic rocks in plateaus (Phuoc Long and Dalat) in Southern Vietnam (Lee et al., 1998). The younger eruptions mainly occurred in the volcanic fields closer to the coast of Vietnam (e.g., Con Co, Ly Son, Xuan Loc, and Iles des Cendres). It is also noted that the volcanism in Central Vietnam had been active for a prolonged period (15 Myrs). The obtained K-Ar ages (Table S3 in Supporting Information S1) range from 7.55 Ma to 0.03 Ma, which falls within the range of previously published dates by the $^{40}Ar/^{39}Ar$ method (Lee et al., 1998) and the K-Ar method (An et al., 2017; Barr & Macdonald, 1981; Hoang et al., 2019; Koszowska et al., 2007; Le et al., 2019; Rangin et al., 1995). Although our data do not span the whole range of ages, the studied samples cover most of the individual volcanic fields from north to south and represent the major volcanic activity in Vietnam in the last 10 Myrs. Details of the ages and volcanic history of each volcanic field are described in Text S4 and Figure S3 in Supporting Information S1.

4.3. Major and Minor Elements

Normative mineral classification of the rock series (Table S2 in Supporting Information S1) is generally consistent with the classification by a total alkali-silica (TAS) diagram (Figure 2a; Irvine & Baragar, 1971). Given that most of the studied samples have a SiO_2 abundance lower than 52 wt% (anhydrous basis), we refer to them as (alkaline or sub-alkaline) basalts. They have $Mg^{\#}$ [$\equiv 100 \times Mg/(Mg + Fe^{2+})$ in molar] < 69 [where Fe^{2+}/Fe_{total} (molar) = 0.85] and Cr < 600 ppm (Figures 2k and 2l); these values are lower than those of primitive basalt magmas ($Mg^{\#} > 70$ and Cr > 1,000 ppm; Green, 1973). Alkaline basalts have higher abundances of Al_2O_3 (Figure 2c), Na_2O (Figure 2h), and K_2O (Figure 2i) than sub-alkaline basalts at a given SiO_2 in general. Major-element compositions of alkaline and sub-alkaline basalts significantly overlap irrespective of sample locations. Exceptions are Na_2O, Ni, and Cr. The alkaline basalts from Buon Ma Thuot and Xuan Loc have higher abundances of these elements than the alkaline basalts from Ly Son-Quang Ngai and Pleiku at given SiO_2 and MgO abundances (Figures 2h, 2k, and 2l).

4.4. Trace Elements

The Vietnamese basalts show enrichments of highly-incompatible elements (e.g., Rb, Th, and light rare-earth elements) relative to the primitive mantle values (McDonough & Sun, 1995), and abundance patterns similar to those of ocean island basalts (OIB, Figure 3). In general, alkaline basalts have higher abundances of incompatible elements than sub-alkaline basalts in the same volcanic field. It is noted that sample CC16.1 from Con Co Island (Figure 3a) displays a striking pattern with depletions of Cs, Rb, and K. With its higher LOI (1.86 wt %), depletions of these elements are due to alteration, and hence the sample is excluded in the following discussion.

Vietnamese basalts commonly show a positive anomaly of Sr and a negative anomaly of Pb (Figure 3). The extents to which these elements are enriched or depleted are expressed as $Sr/Sr^* [Sr_N/(Ce_N \times Nd_N)^{0.5}$ where subscript N denotes normalized element abundance] and $(Pb/Ce)_N$ (Figure 4a). The Sr/Sr* and $(Pb/Ce)_N$ ratios of the basalts are different among the volcanic fields studied here, as was also reported by Hoang et al. (2018). Strontium is more enriched in sub-alkaline basalts from the volcanic fields in Southern Vietnam (Buon Ma Thuot, Phuoc Long, Xuan Loc, and Phu Quy Island), whereas Pb is more enriched in sub-alkaline basalts from the volcanic fields in Central Vietnam (Con Co, Ly Son-Quang Ngai, and Kong Plong; Figure 4a). The extents of Th and Nb anomalies are also different among these basalts (Figures 3 and 4b); sub-alkaline basalts in Central Vietnam are more enriched and depleted in Th and Nb, respectively, than sub-alkaline basalts in Southern Vietnam. Alkaline basalts in Central and Southern Vietnam show similar Sr, Pb, Nb, and Th enrichments. Note that the assemblages and abundances of phenocrysts are not systematically different in sub-alkaline basalts from Central and Southern Vietnam (Text S3 and Figure S2 in Supporting Information S1). Hence the different extents of enrichments or depletions in Sr, Pb, and Th are considered to be intrinsic features of the parental magmas. Trace-element compositions of seafloor basalts from the EVS/SCS spreading ridges reveal that two types of parental magmas were erupted in this marginal basin (Figure S4 in Supporting Information S1), as was suggested by Zhang, Luo, et al. (2018). Basalts from the site U1431 show an abundance pattern similar to N-MORB (Gale et al., 2013), except for alkalis (Cs, Rb, and K) and Pb. Enrichments of alkalis are probably due to seafloor alteration. Basalts

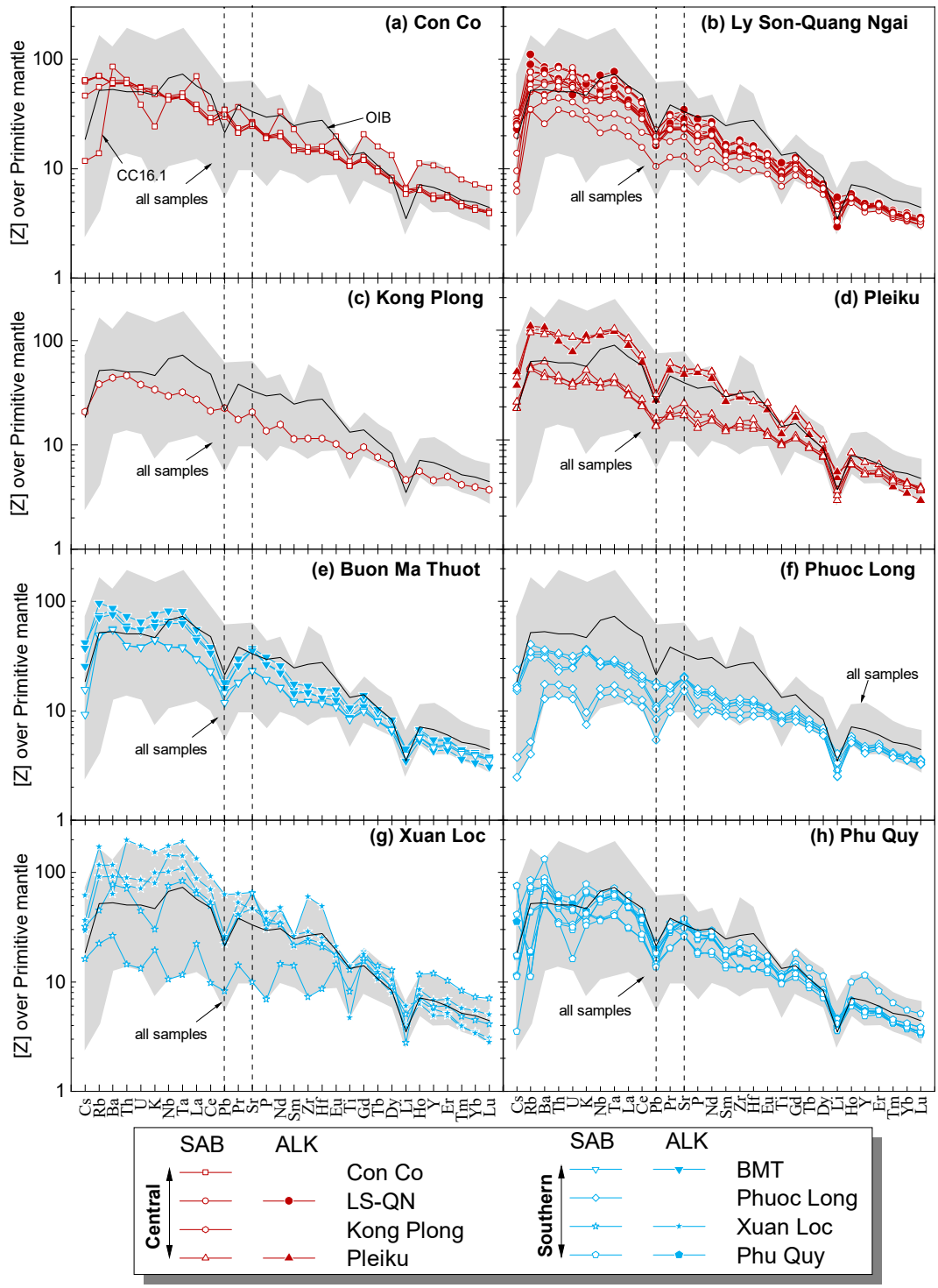

Figure 3. Trace-element abundances ([Z]) normalized to the primitive mantle (McDonough & Sun, 1995); (a) Con Co, (b) Ly Son-Quang Ngai (or LS-QN), (c) Kong Plong, (d) Pleiku, (e) Buon Ma Thuot (or BMT), (f) Phuoc Long, (g) Xuan Loc, (h) Phu Quy Island. Red, Central Group; pale blue, Southern Group. Alkaline (ALK) and sub-alkaline (SAB) series are denoted as filled and open symbols, respectively. The line denoted as OIB shows the abundance pattern of average intraplate-oceanic alkaline basalts (Sun & McDonough, 1989).

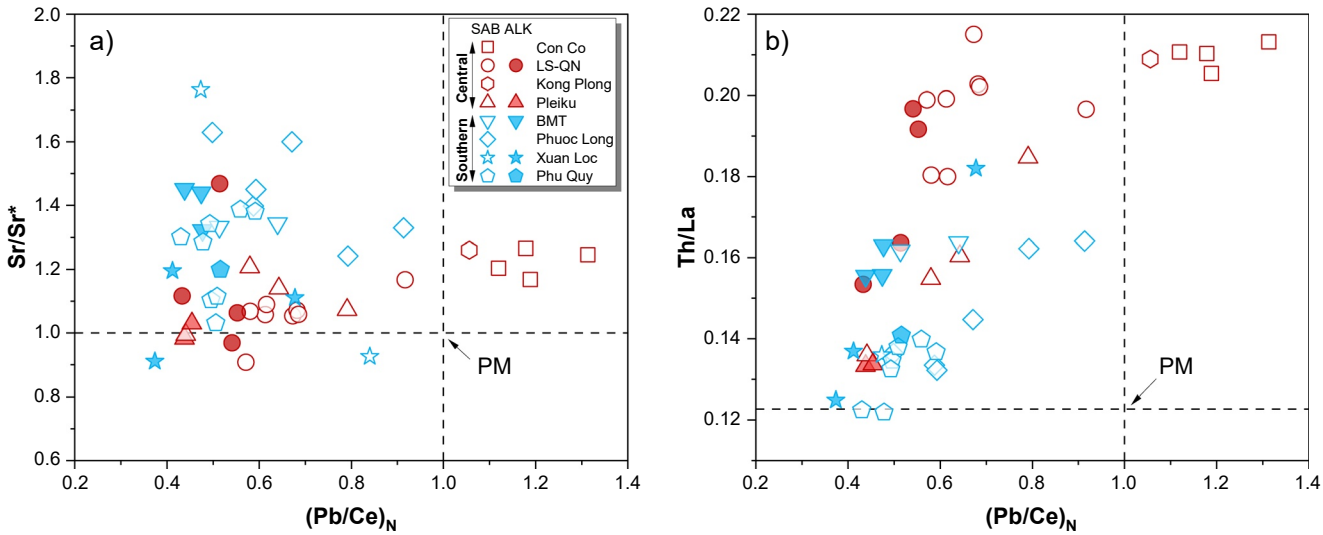

Figure 4. Covariations of trace-element ratios of Vietnamese basalts. (a) $(Pb/Ce)_N$ against Sr/Sr* which are calculated as $Sr/Sr^* = Sr_N/(Ce_N \times Nd_N)^{0.5}$, where the subscript *N* indicates normalization to primitive mantle (PM, McDonough & Sun, 1995). (b) $(Pb/Ce)_N$ against Th/La. The horizontal and vertical dashed lines denote $(Pb/Ce)_N$, Sr/Sr* and Th/La of PM. Abbreviations of the Vietnamese volcanic fields: BMT, Buon Ma Thuot; LS-QN, Ly Son-Quang Ngai.

from the site U1433 have greater abundances of Ba, Th, U, Nb, Ta, La, and Ce than the basalts from the site U1431 (Text S5 and Figure S4 in Supporting Information S1).

4.5. Sr-Nd-Pb Isotopes

The studied basalts show large variations in Sr, Nd, and Pb isotopic compositions (Figure 5), and cover the entire range of basalts from previous studies (An et al., 2017; Hoàng et al., 2013; Hoang et al., 1996, 2018, 2019). Alkaline and sub-alkaline basalts in the same volcanic fields show isotopic compositions considerably overlapping each other. Instead, the studied basalts show a regional difference (Figures 5b–5d, Figure S5 in Supporting Information S1); the basalts from Central Vietnam (13.5–17.2°N; denoted as Central Group) mostly have higher $^{206}Pb/^{204}Pb$ ratios than the basalts from South Vietnam (10.5–13.5°N; denoted as Southern Group). The Pb isotope data of these two groups, obtained by double-spike methods in this study, appear to form linear arrays with different slopes in $(^{206}Pb/^{204}Pb)_i$-$(^{207}Pb/^{204}Pb)_i$ and $(^{206}Pb/^{204}Pb)_i$-$(^{208}Pb/^{204}Pb)_i$ plots (Figures 5c and 5d). Only an alkaline basalt deviates from these arrays; that is from Buon Ma Thuot, and has a significantly high $^{143}Nd/^{144}Nd$ ratio and low $^{206}Pb/^{204}Pb$ ratio similar to EVS/SCS basalts. The existence of two Pb-isotope arrays becomes less clear when data in the previous studies (An et al., 2017; Hoang et al., 1996, 2018, 2019; Hoàng et al., 2013) are included in a plot of $(^{206}Pb/^{204}Pb)_i$-$(^{207}Pb/^{204}Pb)_i$, presumably due to inadequate correction of mass bias effect by conventional techniques (e.g., Baker et al., 2004; Pineda-Velasco et al., 2015; Thirlwall, 2000). It should be noted that Hoang et al. (2018) divided differently the volcanic field in Vietnam as Central Group, South-Central Group, and Southern Group, respectively, based on distinct trace-element characteristics. The borders of these groups are located at 14°N (Central vs. South-Central) and 12°N (South-Central vs. Southern), respectively. The South-Central Group by Hoang et al. (2018) is a transitional zone of their Central and Southern Groups. The border of our Central and Southern Groups, located at 13.5°N, is within this transitional zone.

To substantiate the regional Pb-isotopic difference, we performed the statistics *F* test to find the likelihood that two groups are drawn from the same distribution (the null-hypothesis). Specifically, residual variances of regression lines in the $(^{206}Pb/^{204}Pb)_i$-$(^{207}Pb/^{204}Pb)_i$ and $(^{206}Pb/^{204}Pb)_i$-$(^{208}Pb/^{204}Pb)_i$ plots are compared between those calculated for pooled data and those calculated individually for Central and Southern Groups. If residual variances of individual regressions are significantly smaller than that for pooled data, the null hypothesis is rejected. In other words, the Central and Southern Groups form different isotopic populations. Details about the *F* test are described in Text S6, and the results of *F* test performed on the Pb isotope data are shown in Table S5 in Supporting Information S1. Comparison of the combined residual sum of squares for individual regressions with a pooled regression results in the statistic *F* values of 25.65 and 13.12 for $(^{206}Pb/^{204}Pb)_i$-$(^{207}Pb/^{204}Pb)_i$ and

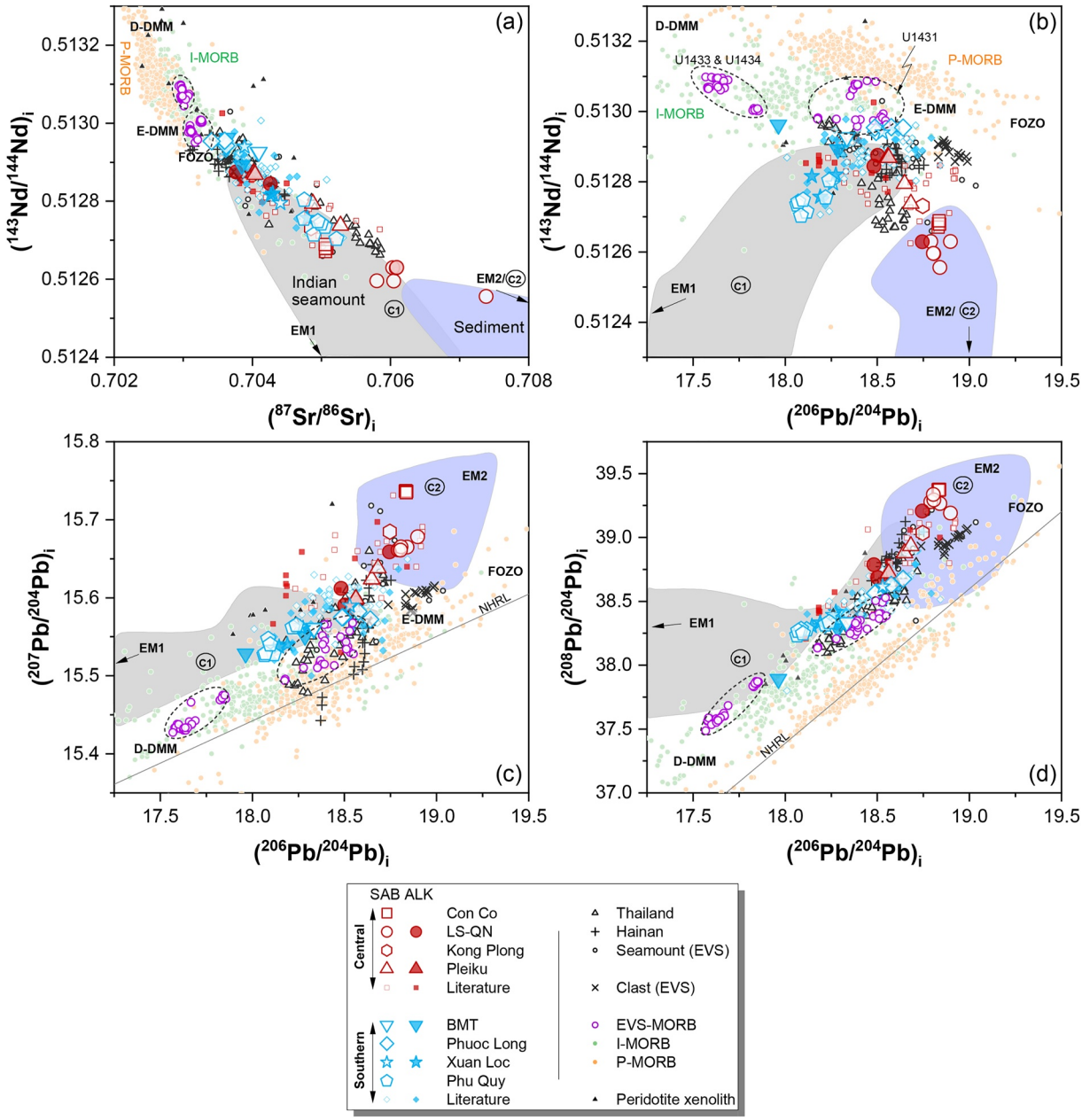

Figure 5. Plots of (a) $(^{87}Sr/^{86}Sr)_i$ versus $(^{143}Nd/^{144}Nd)_i$, (b) $(^{206}Pb/^{204}Pb)_i$ versus $(^{143}Nd/^{144}Nd)_i$, (c) $(^{206}Pb/^{204}Pb)_i$ versus $(^{207}Pb/^{204}Pb)_i$, and (d) $(^{206}Pb/^{204}Pb)_i$ versus $(^{207}Pb/^{204}Pb)_i$. For comparison, literature data for Cenozoic mafic volcanic rocks in Vietnam and the adjacent regions are also shown; Vietnam (An et al., 2017; Hoang et al., 1996, 2018, 2019; Hoàng et al., 2013), Thailand (Mukasa et al., 1996; Yan et al., 2018; Zhou & Mukasa, 1997), Hainan (Wang et al., 2013), EVS/SCS [seamount, Tu et al. (1992); Yan et al. (2008); clast, Zhang et al. (2017); seafloor basalts (EVS/SCS-MORB), Zhang, Luo, et al. (2018); Zhang, Sun, et al. (2018)]. Isotopic ratios are age-corrected (denoted as subscript i; Table S1). Also shown are isotopic compositions of seamount basalts (denoted as "Indian seamount") from Eastern Wharton Basin Volcanic Province (Figure 10a; Hoernle et al., 2011), seafloor basalts in Indian and Pacific Oceans (I-MORB and P-MORB, Gale et al., 2013), and (seafloor) sediment (Gasparon & Varne, 1998; Ben Othman et al., 1989; Plank & Langmuir, 1998). Isotopic compositions of peridotite xenoliths in Vietnamese basalts are from Anh et al. (2020), Huong and Hoang (2018), and Nguyen and Kil (2020). The circles labeled C1 and C2 are hypothetical end-member components proposed in this study to explain isotopic variability in mafic volcanic rocks in Vietnam and the adjacent regions (Text S7 in Supporting Information S1 and Table S6). Data sources for the compositions of mantle end-member components are as follows: D-DMM and E-DMM, Workman and Hart (2005), except for $^{208}Pb/^{204}Pb$ of D-DMM that is from Salters and Stracke (2004); EM1 and EM2, Zindler and Hart (1986); FOZO, Stracke et al. (2005). Analytical uncertainties of our data are smaller than the symbols. ALK and SAB indicate alkaline and sub-alkaline basalts, respectively. NRHL is the Northern Hemisphere Reference Line (Hart, 1984). Abbreviations of the Vietnamese volcanic fields: BMT, Buon Ma Thuot; LS-QN, Ly Son-Quang Ngai.

$(^{206}Pb/^{204}Pb)_i$-$(^{208}Pb/^{204}Pb)_i$ relationships, respectively. These values are much greater than the critical F value at 1% ($F = 5.29$) or even 0.1% ($F = 8.52$) significance levels. The null hypothesis probabilities for F values of 25.65 and 13.12 are 2×10^{-5} and 0.006%, respectively, indicating that the null hypothesis can be rejected at much better than 99% confidence. We also performed an F-test for data from this study and that compiled from the previous studies (An et al., 2017; Hoang et al., 1996, 2018, 2019; Hoàng et al., 2013). The statistic F values are 0.34 and 11.56 for $(^{206}Pb/^{204}Pb)_i$-$(^{207}Pb/^{204}Pb)_i$ and $(^{206}Pb/^{204}Pb)_i$-$(^{208}Pb/^{204}Pb)_i$ relationships, respectively. The critical F value at 1% and 0.1% significant levels are 4.7 and 7.2, respectively.

The result holds two important implications: (a) it confirms the existence of two Pb-isotope subpopulations in Vietnamese basalts based on the significant statistic F for $(^{206}Pb/^{204}Pb)_i$-$(^{208}Pb/^{204}Pb)_i$ from our data and from the literature data and (b) it implies the analytical problem of $^{207}Pb/^{204}Pb$ in the literature data based on significant difference in the statistic F for $(^{206}Pb/^{204}Pb)_i$-$(^{207}Pb/^{204}Pb)_i$ from our data ($F = 25.65$) and from the literature data ($F = 0.34$, i.e., significantly smaller that critical F).

These two groups also show differences in Sr and Nd isotopic compositions (Figures 5a and 5b). The $^{87}Sr/^{86}Sr$ ratios of the Central Group basalts extend from 0.7038 to more radiogenic compositions (0.7074), whereas those of the Southern Group basalts show a smaller variation and less radiogenic compositions (0.7034–0.7052). The $^{143}Nd/^{144}Nd$ ratios are inversely correlated with $^{87}Sr/^{86}Sr$ ratios, and the Central and Southern Group basalts apparently form a single linear array. Within the Southern Group, the $^{143}Nd/^{144}Nd$ ratios become more radiogenic in basalts from south to north, whereas such spatial variation in $^{143}Nd/^{144}Nd$ ratio is not observed in the Central Group.

The Sr and Nd isotopic data of EVS/SCS basalts ($^{87}Sr/^{86}Sr$ = 0.7029–0.7032 and $^{143}Nd/^{144}Nd$ = 0.51298–0.51309) are comparable to the previously published data (Figure S6 in Supporting Information S1, Table S1; Zhang, Luo, et al., 2018; Zhang, Sun, et al., 2018). The EVS/SCS basalts are characterized by lower $^{87}Sr/^{86}Sr$ and $^{206}Pb/^{204}Pb$ (17.5–18.6) and higher $^{143}Nd/^{144}Nd$ than those of basalts in subaerial volcanic fields in Vietnam (Figures 5a and 5b). Within the EVS/SCS, basalts from different collection sites show a clear isotopic distinction. Basalts from the sites U1433 and U1434, located in the central basin of EVS/SCS, show the isotopic composition akin to D-DMM (Workman & Hart, 2005) whereas basalts from the Site U1431, located on the seamount (a part of Scarborough seamount chain), have the isotopic composition similar to E-DMM (Workman & Hart, 2005).

5. Discussion

We examine possible factors that control the geochemical compositions of mafic volcanic rocks in Vietnam; those are (a) post-melting processes that modify geochemical compositions of mantle-derived magmas, (b) melting processes which produce a large range of primary magmas with variable compositions, and (c) lithological and geochemical characteristics of the sources of parental magmas of the Vietnamese basalts.

5.1. Post-Melting Processes

It is generally expected that mantle-derived magmas react, to some extent, with crustal materials during their ascent. The crust of subaerial volcanic fields in Vietnam is dominated by mafic rocks in its lower part, and by intermediate and felsic rocks in its upper part (Yu, Y. et al., 2017b). Among these crustal lithologies, upper-crustal felsic rocks are considered to be a dominant assimilant as they have lower solidus (650–900°C; Sawyer et al. [2011]) and higher abundances of incompatible elements (Jiang et al., 2020; Lan et al., 2003; Nguyen, Satir, Siebel, Vennemann, & Van Long, 2004; Nguyen, Satir, Siebel & Chen, 2004; Owada et al., 2007; Shellnutt et al., 2013). Crustal assimilation cools the magma and leads to crystallization, whereas the latent heat of fractional crystallization promotes assimilation. Such positive feedback is governed by mass- and energy-transfer processes. We examine such processes using the Magma Chamber Simulator (MCS); the MCS is a mass- and energy-balanced, the thermodynamic tool that allows for the investigation of open-system magmatic processes (Bohrson et al., 2014, 2020; Heinonen et al., 2020). For the modeling undertaken here, the least differentiated alkaline basalts in each volcanic field ($Mg^{\#} \geq 58$) were chosen as a common parental magma (Figure 6). Two possible assimilants are examined; one is a Paleozoic–Mesozoic granitic rock from the Kontum massif in Central Vietnam (Text S1 in Supporting Information S1; Jiang et al. [2020]; Lan et al. [2003]; Owada et al. [2007]), and the other is a Cretaceous granitic rock from the Dalat zone in Southern Vietnam (Text S1; Nguyen, Satir, Siebel, Vennemann, and Van Long [2004]; Nguyen, Satir, Siebel and Chen [2004]; Shellnutt et al. [2013]). The reaction

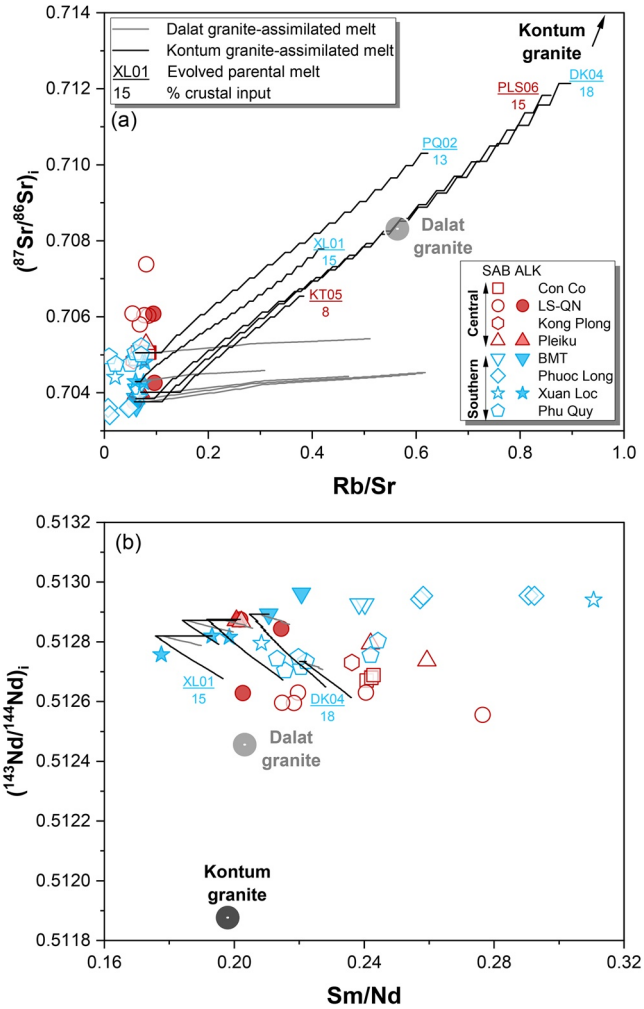

Figure 6. (a) $(^{87}Sr/^{86}Sr)_i$ against Rb/Sr, (b) $(^{143}Nd/^{144}Nd)_i$ against Sm/Nd. The AFC (assimilation and fractional crystallization) model was performed using the Magma Chamber Simulator (MCS; Bohrson et al., 2014; Bohrson et at., 2020; Heinonen et al., 2020). The least differentiated basalts from each volcanic field were chosen as parental magmas, and the calculated compositions of daughter magmas are shown by black and gray lines. Black lines represent the evolution of daughter magmas via assimilantion of a granitic rock of the Kontum massif (00041904A; Owada et al., 2007) in Central Vietnam. Gray lines represent the evolution of daughter magmas via assimilation of a granitic rock of the Dalat zone (SVN7C; Shellnutt et al., 2013) in Southern Vietnam. All input parameters used in the model are provided in Text S8 in Supporting Information S1 and Table S7. Abbreviations of the Vietnamese volcanic fields: BMT, Buon Ma Thuot; LS-QN, Ly Son-Quang Ngai.

between parental magma and assimilant is assumed to have occurred in the crustal magma reservoir (0.2 GPa). The H_2O and CO_2 contents of the parental magmas are estimated by the indirect approach (discussed in Section 5.3). The temperature of an assimilant before interaction with magma is assumed to be 400°C from the crustal geotherm beneath Vietnam (Yu, C. et al., 2017). Details of the model inputs are provided in Text S8 and Table S7 in Supporting Information S1.

Results of the modeling are shown in Figure 6. The model predicts that differentiated magmas evolve to have a large variation in Rb/Sr without a significant variation in Sm/Nd (given as solid lines in Figures 6a and 6b). The predicted changes in Rb/Sr (0.06–0.90) and Sm/Nd (0.21–0.23) are at odds with data obtained for Vietnamese basalts, showing a large variation in Sm/Nd (0.20–0.30) and fairly constant Rb/Sr (0.01–0.10). Accordingly, the majority of the studied samples do not follow the trend for assimilation. We thus consider that the observed compositional variability is an intrinsic feature of parental magmas. Below, we discuss the processes that occurred at subcrustal depths, that is, lithology of magma sources, melting processes, and the variability in the composition of the magma sources.

5.2. Lithology of Magma Sources

Recent studies suggested the presence of mafic lithologies (pyroxenite or eclogite) in the source of parental magmas of basalts in Vietnam (An et al., 2017; Hoang et al., 2018) and EVS/SCS (Zhang et al., 2018b). These studies examined abundances of major and minor elements in olivine phenocrysts; specifically, they noted abundances of Ni higher than, and those of Ca and Mn lower than olivines in MORB at given Fo content [≡ 100 × Mg/(Mg + Fe) in molar]. Such elemental features have been interpreted as evidence that melts equilibrated with an olivine-free, pyroxene- (and garnet-) bearing source, that is, pyroxenite (Sobolev et al., 2005).

However, recent experimental studies documented that the partitioning of Ni, Ca, and Mn between melt and residual peridotite varies significantly, owing to changes in pressure and temperature or residual phase assemblages during melting (Matzen et al., 2017). Magmatic processes are also responsible for the abundances of these elements in olivine: re-equilibration of olivine with recharged magma results in the elevation of Ni and the decrease of Mn abundances by cation diffusion (Gleeson & Gibson, 2019). Furthermore, an increase in the abundance of H_2O and CO_2 in a magma leads to a decrease in the abundance of Ca within olivine due to the combined effect of (a) reducing Ca activity in the melt by bonding of hydrous or carbonate species on Ca-complexes and (b) depletion of Ca in the melt by enhanced clinopyroxene crystallization (Feig et al., 2006; Gavrilenko et al., 2016). It is therefore considered that distinct Ni, Ca, and Mn abundances of olivines from those in MORBs do not readily indicate that a magma that contains olivines with high-Ni, low-Ca or low-Mn abundances was derived from olivine-free mafic lithology.

We examined the existing data for major- and minor-element compositions of olivine phenocrysts in the Vietnamese basalts (An et al., 2017; Hoang et al., 2018; Text S9.1 and Figure S7 in Supporting Information S1). The Ni abundance of high-Mg olivine phenocrysts (Fo = 88 or greater) ranges from 2000 to 3300 ppm, being well within the range of Ni abundance in olivines crystallized from peridotite partial melts (Sobolev et al. [2007]; see Figures S7a and S7b in Supporting Information S1). The Ca abundance of olivines is consistent with that estimated from the partition coefficient between olivine and melt ($D^{olivine/melt}$) for hydrous systems (Gavrilenko et al., 2016); a magma containing 0–4 wt% H_2O or 1–2 wt% CO_2 could crystallize olivines with the Ca abundance observed in

phenocrysts in the Vietnamese basalts (Figure S7d in Supporting Information S1). These H_2O and CO_2 abundances are consistent with those estimated by the other independent approaches (discussed in Section 5.3).

Another recent study (Qian et al., 2021) also found geochemical characteristics which support the insignificant role of a pyroxenite source for the basalts from EVS/SCS seamounts. The study reported that olivine phenocrysts in basalts from EVS/SCS seamounts have a Ni abundance lower than those in Vietnamese basalts, but comparable to those found in MORB, yet the basalts from these two regions share common trace-element and isotopic characteristics. They simply attributed the higher Ni abundances and lower Mn abundances of olivine phenocrysts in Vietnamese basalts to high-pressure melting of a magma source and subsequent low-pressure crystallization of a magma (Matzen et al., 2017). Higher-pressure melting leads to the production of primary magma with higher Mg, higher Ni, and lower Mn abundances than those produced at lower pressure. Subsequently, such a magma ascends to a shallow level and crystallizes olivine phenocrysts. At that depth, olivine phenocrysts sequester more Ni and less Mn due to increasing $D_{Ni}^{olivine/melt}$ and decreasing $D_{Mn}^{olivine/melt}$ with decreasing pressure (Matzen et al., 2017). Consequently, olivine phenocrysts in Vietnamese basalts that erupted on thicker lithosphere could have higher Ni and lower Mn abundances than olivine phenocrysts in EVS/SCS seamounts where the lithosphere is thinner.

An et al. (2017) argued that major-element compositions of Vietnamese basalts, corrected for the effect of fractional crystallization, fall within the range of experimental melts from silica-deficient eclogite (Dasgupta et al., 2010). However, the calculated compositions in An et al. (2017), as well as the compositions calculated for our samples (see Section 5.3), are also well within the range of melts produced by partial melting of peridotite (Text S9.2 and Figures S8 and S9 in Supporting Information S1). We also examined whole-rock major-element characteristics by the approach of Yang et al. (2019) who defined the parameter called FCKANTMS which allows the origin of melts to be determined. The FCKANTMS is an acronym for the oxide components used to derive this parameter (FeO, CaO, K_2O, Al_2O_3, Na_2O, TiO_2, MgO, and SiO_2). For its derivation, log ratio transformation is employed [ln(FeO/CaO), ln(K_2O/Al_2O_3), ln(TiO_2/Na_2O), ln(Na_2O/K_2O), ln(Na_2O/TiO_2) and ln(MgO/SiO_2)], and then these log ratios are summed after multiplying empirical factors. The empirical factors are defined so as to adjust the FCKANTMS value for fertile-peridotite melts to be 0. It is noted that the FCKANTMS value is little affected by olivine fractionation. Whereas, this value significantly increases by removal of clinopyroxene from a melt. In other words, a primary basalt with the FCKANTMS value $\gg\gg 0$ is considered to have been derived from a mafic lithology (e.g., pyroxenite). Yang et al. (2019) gave the threshold values of 0.05 ± 0.10 for discrimination of peridotite versus transitional (olivine-rich mafic) lithology and 0.37 ± 0.08 for discrimination of transitional lithology versus (olivine-poor) mafic lithology. The latter threshold value marks the upper limit of FCKANTMS for melts of peridotitic sources.

The Vietnamese basalts (samples with MgO >8 wt%) yield an average FCKANTMS value of 0.27 (ranging from −0.04 to 0.50) and the majority of these samples have FCKANTMS values lower than 0.37 (Figure S9c in Supporting Information S1). This result suggests that the source of the Vietnamese basalts is dominated by olivine-bearing mafic to ultramafic lithology. There is no convincing evidence for the significant contribution of an olivine-free lithology (eclogite or silica-excess pyroxenites) in the production of basaltic magmas in Vietnam. We agree with the statement of Matzen et al. (2017): "the standard (and far simpler and better constrained) reference model based on partial melting of fertile peridotite as a dominant process contributing to basaltic melt worldwide". In the next section, we apply a thermobarometric approach, based on experimental peridotite melting, to Vietnamese basalts, which can yield reliable estimates of melting conditions.

5.3. Melting Processes

Experimental studies demonstrated that melting of mafic or ultramafic rocks in the mantle produce melts with variable compositions under a range of pressures (P) and temperatures (T) (e.g., Hirose, 1997; Hirschmann et al., 2003). Hence the P-T conditions of melting can be examined by inverse modeling using the major-element composition of primitive basaltic rocks.

We applied the following approaches: (a) select the samples with minimal fractional crystallization, (b) correct the effect of fractional crystallization and estimate the primary magma compositions, and (c) apply thermobarometry. For Approach 1, the least differentiated samples with a liquidus phase of only olivine were selected based on CaO/Al_2O_3 ratios (Figure S8 in Supporting Information S1). The majority of basalts with MgO >7.5 wt% have CaO/Al_2O_3 ratios falling within the range of experimental peridotite melts (Condamine et al., 2016;

Davis et al., 2011; Davis & Hirschmann, 2013; Falloon & Danyushevsky, 2000; Hirose & Kawamura, 1994; Hirose & Kushiro, 1993, 1998; Kushiro, 1996; Pickering-Witter & Johnston, 2000; Walter, 1998), indicating that the basalts were affected minimally by crystallization of clinopyroxene and plagioclase (e.g., Liu et al., 2015). To further avoid the spurious influence of fractionation correction, we selected rocks with MgO >8 wt%. For Approach 2, equilibrium olivine was incrementally added until the melt compositions reached equilibrium with the mantle containing olivine with Fo [$\equiv 100 \times Mg/(Mg + Fe^{2+})$] = 90. The use of Fo = 90 is supported by analysis of most magnesian olivine found as phenocrysts in Vietnamese basalts (An et al., 2017). The Fe^{2+}/Fe_{total} in the melt is assumed to be 0.85 based on H_2O abundances (see below) and an empirical function by Kelley and Cottrell (2009), and $(Fe^{2+}/Mg)_{olivine}/(Fe^{2+}/Mg)_{melt}$ is assumed to be 0.3 (Blundy et al., 2020; Roeder & Emslie, 1970).

For Approach 3, we applied the algorithms of Putirka (2008), Lee et al. (2009), Herzberg and Asimow (2015), and Plank and Forsyth (2016). Volatile effects on depression or elevation of solidi of magma sources are also taken into consideration. The abundance of H_2O in primary magma is estimated to be 0.47–2.0 wt % [mean 1.08 (±0.37, 1σ) wt%] from the Ce abundance of calculated primary magmas and the H_2O/Ce ratio is assumed to be 200 (Dixon et al. [2002]; see also Text S10 in Supporting Information S1). Uncertainty of H_2O estimation is 30%. The higher H_2O abundances (1.5–2.0 wt%) are obtained for primary magmas of strongly alkaline basalts from Pleiku (KT05 and KT06) and Xuan Loc (XL01 and XL02). An et al. (2017) also obtained similar H_2O abundances (1.9–2.0 wt%) for Xuan Loc basalts. It is noted that these basalts show overall enrichments of incompatible trace elements (e.g., high Ce/Yb), probably due to a smaller degree of partial melting (discussed below).

Another major volatile may be CO_2 which also affects calculated P and T (Dasgupta et al., 2013; Plank & Forsyth, 2016). We used the empirical equation of Plank and Forsyth (2016) for the correction of the estimated T:

$$\Delta T_{CO_2} = \frac{SiO_2 - 50.3}{0.12 \times (-1.067)} \quad (1)$$

where ΔT_{CO2} represents the deviation of calculated T for a volatile-free basis, and SiO_2 is its abundance in primary magma (in wt%). It is noted that this empirical relationship is applicable to a P-T range of 2–3 GPa. We exclude the results for Xuan Loc basalts since P > 3 GPa. The ΔT_{CO2} for parental magmas of Vietnamese basalts are estimated to be 16–35°C with the estimated CO_2 = 2.2–4.5 wt% (Text S10 and Figure S10 in Supporting Information S1). Uncertainty of CO_2 estimation is 30%. The CO_2 abundances estimated by this approach are significantly higher than those obtained by whole-rock analyses (<2 wt%; Hoang et al. [1996]), possibly due to the loss of CO_2 through degassing during eruptions (Dixon et al., 1997). This inference is supported by the consistency between the estimated CO_2 abundances in primary magmas based on the extent of SiO_2 deficit (CO_2 = 2.2–4.5 wt%) and Ba-Nb abundances in the calculated primary magmas (CO_2 = 1.6–4.9 wt%; Text S10 in Supporting Information S1).

When using the thermometer of Herzberg and Asimow (2015), P by Plank and Forsyth (2016)'s barometer was used, and solidus depression by H_2O follows Putirka (2016). Results of the calculation are summarized in Figure S11 in Supporting Information S1 and Table S8, showing the overall consistency of P-T estimates by different algorithms within ±0.15 GPa and ±35°C. The pressures are lowered by 0.01–0.41 GPa (mean 0.15 GPa) while the melting temperatures are also lowered by 18–53°C (mean 37°C) for melting of the source that contains H_2O and CO_2. Since the estimated P and T are mutually related, the difference in P and T for the cases of volatile-bearing and volatile-free options are 0.02 GPa and 16°C, respectively.

The estimated P-T conditions form a broad continuous array above the dry solidus of peridotite (Hirschmann, 2000), and follow an adiabatic gradient of partially-molten peridotite (T_p = 1450°C, Figure 7; Katz et al. [2003]). This result indicates that the parental magmas of Vietnamese basalts were extracted from the adiabatically upwelling mantle at various depths; in general, parental magmas of sub-alkaline basalts were segregated at shallower depths than parental magmas of alkaline basalts. There is no clear difference in melting P-T for parental magmas from different volcanic fields. The mantle potential temperatures (T_p) were estimated using an adiabatic gradient of solid peridotite (Katz et al., 2003), to be 1380–1490°C with a median T_p = 1440°C (Figure 7), consistent with the results of previous studies (T_p = 1440–1490°C; An et al. [2017]; Hoang & Flower [1998]). The T_p for the Vietnamese basalts partially overlaps with those for Hainan basalts, but the mean T_p of Hainan basalts is higher by 100°C than T_p calculated for this volcanic field (Wang et al., 2012). It should be noted that T_p of Vietnamese basalts does not show a clear correlation with latitude (Figure S12 in Supporting Information S1), suggesting that

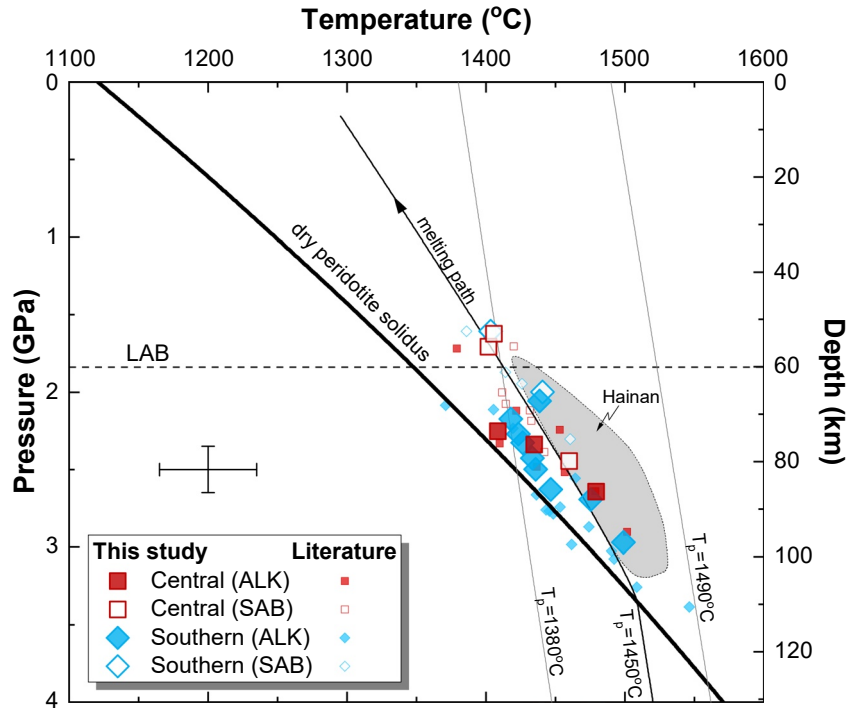

Figure 7. Pressure (P) and temperature (T) of melting for production of Vietnamese basalts, calculated by the algorithms of Plank and Forsyth (2016) and Putirka (2008). Data used for P-T calculation are major-element compositions of the basalts by this study and previous studies (same as in Figure 5). The uncertainty of the estimated pressure and temperature are ±0.15 GPa and ±35°C, respectively. For comparison, the pressure-temperature condition of melting for production of Hainan basalts are shown (Wang et al., 2012). The dry solidus of peridotite, shown by a thick black line, is from Hirschmann (2000). Pressure-temperature gradients of solid and melting peridotites, calculated after Katz et al. (2003), are also shown. The adiabatic gradient of solid peridotite is used to calculate mantle potential temperatures (T_p). The horizontal dashed line labeled LAB denotes the depth of lithosphere-asthenosphere boundary beneath SE Asia (Ball et al., 2021).

the thermal (and chemical) influence of the Hainan plume is unlikely to be the main cause of the volcanism in Vietnam.

We further examine the melting process by trace-element modeling using the REEBOX PRO by Brown and Lesher (2016). The REEBOX PRO is a forward-modeling program that simulates the adiabatic decompression melting of mantle rocks. Input parameters have options of lithologies and compositions of magma sources, P-T condition in relation to lithospheric thickness and T_p, and physical form of melting regime. We assume two end-member models with different source lithologies; (a) peridotite with a trace-element composition of depleted mid-ocean ridge basalt (MORB) mantle (D-DMM, Workman & Hart [2005]) and (b) silica-deficient pyroxenite (MIXG1; Hirschmann et al. [2003]; Kogiso et al. [2003]) with a trace-element composition of the normal MORB (N-MORB; Gale et al. [2013]). The water content in the source is also a critical parameter. The possible range of water in a peridotite is 100–700 ppm based on H_2O in primary magmas and the partition coefficient of H_2O between mantle rock (peridotite or pyroxenite) and melt ($D_{H_2O}^{solid/melt} = 0.008$, Hirschmann [2006]). The mantle potential temperature for modeling is constrained by the result of thermobarometry (T_p = 1450°C, Figure 7). The average lithosphere thickness beneath Vietnam is from seismic studies (60 km, Ball et al. [2021]). The geometry of the melting regime is assumed to be an active residual mantle column, such as that described by Langmuir et al. (1992). The input parameters for the modeling are summarized in Table S9 and the results of modeling are shown in Figure 8.

The majority of the Vietnamese basalts can be explained by the melting of peridotite with various H_2O abundances (100–700 ppm), consistent with the inference that peridotite is predominant as a source of magma based on major-element compositions. Exceptions are those for the basalts from Phu Quy Island, Xuan Loc, and Pleiku. They have Dy/Yb and La/Yb ratios higher than melts produced from peridotite with a melting degree (F) of 0.5%–2%. We consider that the source of magmas could contain a subordinate amount of eclogite (or other mafic

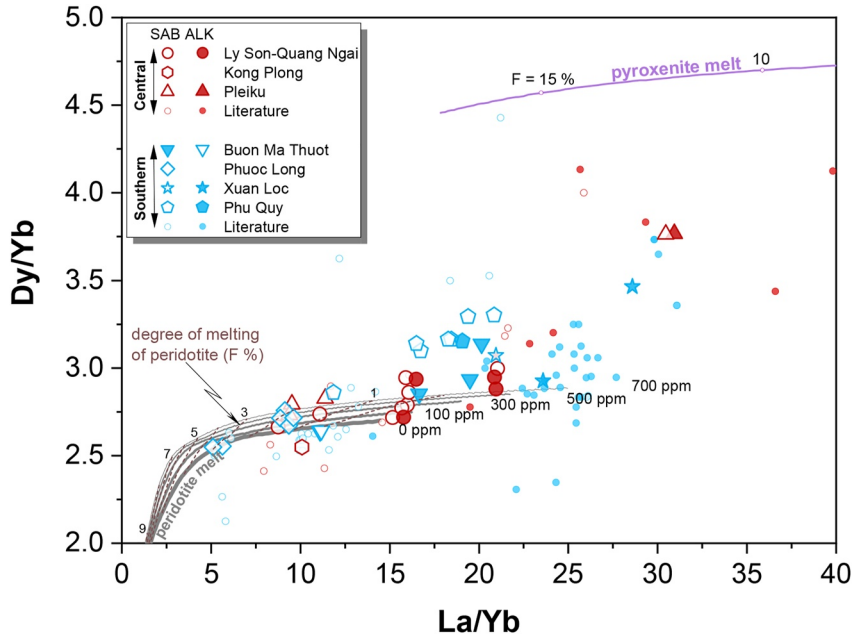

Figure 8. Dy/Yb versus La/Yb of the least differentiated Vietnamese basalts (MgO >7.5 wt% or Mg# > 57). Compositions of melts from peridotite (gray lines) with various amount of H_2O (0–700 ppm) and anhydrous pyroxenite MIX1G (the purple line) at T_p = 1450°C were calculated using the REEBOX PRO (Brown & Lesher, 2016). All the parameters used for modeling are listed in Table S8. Sources of the literature data for basalts from Vietnam are the same as in Figure 5. The abundances of La, Dy and Yb of peridotite are referenced to D-DMM of Workman and Hart (2005) and those of pyroxenite are referenced to N-MORB of Gale et al. (2013).

rocks, such as pyroxenite). In summary, Vietnamese basalts were tapped from the sources at different depths in the mantle consisting of various mafic/ultramafic lithologies. Below, we discuss the origin of these lithologies of magma sources using the Sr, Nd and Pb isotopic compositions of Vietnamese basalts.

5.4. Isotopic Characteristics of Magma Sources

The variations in the Sr-Nd-Pb isotopic compositions of Vietnamese basalts are significantly large. The signal-to-noise ratio (S/N), defined as $(\sigma^2_{obs}/\sigma^2_{err} - 1)^{1/2}$ where σ_{obs} is the observed isotopic variability and σ_{err} is the analytical uncertainty, is much greater than unity; 29 for $^{87}Sr/^{86}Sr$, 6 for $^{143}Nd/^{144}Nd$, 95 for $^{206}Pb/^{204}Pb$, 34 for $^{207}Pb/^{204}Pb$, and 74 for $^{208}Pb/^{204}Pb$. Given that the isotopic ratios are unaffected by melting, a reasonably large S/N supports the involvement of multiple end-member components in the source of the parental magmas of Vietnamese basalts (Figure 5 and Table S6 in Supporting Information S1). One of these end-member components is represented by basalt in Buon Ma Thuot and EVS/SCS basalts. Some EVS/SCS basalts from the sites U1433 and U1434 show Sr-Nd-Pb isotope compositions comparable to D-DMM of Workman and Hart (2005). Major- and trace-element compositions of these EVS/SCS basalts are also well within the range of global normal (N)-MORBs (Qian et al., 2021; Zhang, Luo, et al., 2018; Figure S4 in Supporting Information S1). EVS/SCS basalts from the site U1431 plot on a radiogenic extension of Pb-isotopic array formed with those from the sites U1433 and U1434 (Figure 5). The observed isotopic variations in EVS/SCS are interpreted as the mixing of two end-member components. Zhang, Luo, et al. (2018) attributed compositional variations of EVS/SCS basalts to the mixing of melts derived from the mantle similar to the source of N-MORB and that from the lower continental crust (LCC), whereas Qian et al. (2021) ascribed it to mixing of melts derived from mantle similar to the source of N-MORB and that from recycled young oceanic crust. In either scenario, the isotopically-depleted source is considered to represent the uppermost asthenospheric mantle dominated by refractory peridotite.

Subaerial basalts in Vietnam demonstrate involvement of the other two end-member components, similar in composition to EM1 and EM2 (Zindler & Hart, 1986); the former largely contributes to the Southern Group basalts, while the latter contributes to the Central Group basalts. In other words, regional variation in the isotopic compositions of Vietnamese basalts is dominantly controlled by relative contributions of EM1-and EM-2-like

sources. It has been suggested that EM1-and EM2-like sources have also contributed to Cenozoic basalts in other regions of East Asia (Choi et al., 2008; Flower et al., 2001). Below, we examine the origins of EM1-and EM2-like end-member components having contributed to basaltic magmatism in Vietnam.

The lithospheric origin of EM1-and EM2-like components (Hoang et al., 1996) is ruled out as the isotopic compositions of lithosphere-derived xenoliths in Vietnamese basalts are distinctly different from the compositions postulated for these end-member components (Figure 5; Anh et al., 2020; Huong & Hoang, 2018; C. Nguyen & Kil, 2020). Alternatively, subducted sediments have been considered sources of EM1 and EM2-like components (Kuritani et al., 2011). Sediments are generally enriched in Rb, Pb, U, and Th (Plank, 2005; Plank & Langmuir, 1998) and have variable Rb/Sr, U/Pb, and Th/U ratios due to subsequent diagenesis or subduction metamorphism. Accordingly, subducted sediments could have evolved to possess EM1-or EM2-like isotopic signatures (Stracke et al., 2003). The Southern Group basalts with EM1-like isotopic features do not have elevated Pb/Ce and Th/La (Figure 4). Instead, they show Nb enrichment, which is a contrasting feature to sediments (Figure 3). Hence, their origin from sediment recycling is unlikely.

We noted that the Southern Group basalts exhibit enrichments of Sr (Figures 3 and 4), although these basalts do not show accumulation of plagioclase phenocrysts (Section 4.1). Such features are referred to as "ghost plagioclase signature" and the magmas with this signature are attributed to the melting of mafic lithologies that had plagioclase as a major constituent in their protoliths (e.g., gabbro; Gasperini et al., 2000; Sobolev et al., 2000). It has been proposed that a significant amount of gabbroic rocks, in the form of oceanic plateaus or seamounts (Cloos, 1993), have been subducted into the mantle, and contributed to intraplate magmatism (Gasperini et al., 2000). We consider that subducted seamounts in the Indo-Australian plate are the source of EM1-like components in the Southern Group basalts. Among basalts from seamounts on the Indo-Australian plate, those from the Eastern Wharton Basin Volcanic Province have isotopic compositions consistent with the source of the EM1-like component (Figures 5 and 10a; Hoernle et al. [2011]). These seamounts are currently migrating toward the Indochina Peninsula, suggesting that subducted Indian Oceanic lithosphere may also contain seamounts which could have been an EM-1 source for the Southern Group basalts.

A greater contribution of the EM2-like component is found in some basalts of the Central Group (Con Co Island and Ly Son-Quang Ngai) as well as basalts in adjacent volcanic fields. It is noted that the EM2-type basalts dominantly occur in the northeastern region of the Indochina Peninsula (Northern Vietnam and Hainan) and the EVS/SCS (Figure 5; Hoang et al., 1996; Qian et al., 2021; Tu et al., 1992; Wang et al., 2013; Yan et al., 2008; Zhang, Luo, et al., 2018; Zhang, Sun, et al., 2018). This component is characterized by high Pb/Ce and Th/La ratios (Figure 4) and high time-integrated Rb/Sr and Th/U ratios (Figure 5). We consider that a sediment origin for this component best explains such geochemical and isotopic features. The isotopic composition of this component, estimated from linear arrays in Sr-Nd-Pb isotopic correlation diagrams for Central Vietnam basalts, is well within the range of present-day ocean-floor sediment (Figure 5; Ben Othman et al. [1989]; Gasparon & Varne [1998]; Plank & Langmuir [1998]). The earlier studies for the basalts in Central Vietnam (An et al., 2017; Hoang et al., 2018) and the other volcanic fields adjacent to Central Vietnam (SE China and EVS/SCS; Y.-Q. Li et al. [2020]; Qian et al. [2021]) also estimated a similar composition for this component.

We consider that subducted sediments have been derived from the Pacific Ocean. Y.-Q. Li et al. (2020) suggested based on forward modeling that the EM2-like isotopic composition is attained by the storage of Pacific sediments in the mantle for 100 Myrs or shorter. The volcanic fields in Vietnam are located far (*c*. 1,800 km) from the trench where the Pacific plate is subducting. Nevertheless, transport of the sediment signature to the mantle beneath Vietnam is feasible. The metamorphic equivalent of subducted sediment is stable under deep-mantle *P-T* conditions (Irifune et al., 1994). Subducted sediments could survive in the convecting mantle over the time scales required for recycling. Several studies have documented the occurrence of mantle-derived magmas with the geochemical signature of sediment in the region far from the trench (Kuritani et al., 2011; Murphy et al., 2002).

5.5. Implication for the Origin of Mantle Heterogeneity Beneath Indochina Peninsula

We reaffirm that the isotopic variability of Vietnamese basalts is largely derived from heterogeneity in the asthenospheric mantle beneath Vietnam. Recently, Hoang et al. (2018) proposed that mantle heterogeneity beneath Vietnam is produced by entrainments of various lithologies present within the subducted Pacific plate into the rising Hainan plume. They ascribed spatial variation in the geochemistry of Vietnamese basalts to lateral heterogeneity

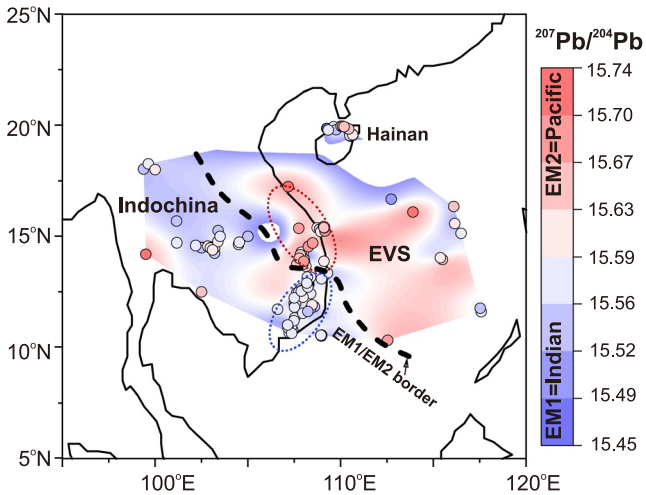

Figure 9. Spatial isotopic variation in $^{207}Pb/^{204}Pb$ ratios of Cenozoic basalts from Indochina Peninsula in SE Asia. Circles denote the localities of basaltic samples of this study and previous studies (sources of literature data are the same as for Figure 5). Color of circle corresponds to $^{207}Pb/^{204}Pb$ values, which indicate relative contributions of EM1 or EM2 sources. The EM1 and EM2 sources are considered to have been originated from the subducted Indian and Pacific oceanic lithospheres, respectively. Two mantle domains, enriched in EM1 or EM2 sources, are roughly divided by the border shown as a bold broken line. Ellipses outlined by red and blue dashed lines denote distributions of two different isotopic subpopulations (i.e., EM1 and EM2 types) in Vietnamese basalts, corresponding to Central and Southern Groups, respectively.

of the mantle by different amounts of entrainments of sediments, basalts, and gabbros, which were disaggregated from the subducted Pacific plate. We also reaffirmed that Central Vietnam basalts possess isotopic characteristics consistent with the involvement of materials consisting of the subducted Pacific plate. However, this scenario cannot solely explain the production of basalts with an EM1-isotopic feature, found in Southern Vietnam; neither young, subducted basalt nor sediments of the Pacific plate have isotopic compositions consistent with an EM1-type source (Figure 5). As discussed in Section 5.4, the involvement of materials consisting of the Indo-Australian plate can account for the EM-1 isotopic feature of Southern Vietnam basalts (Figure 5).

The subduction of two oceanic plates may have produced different isotopic provinces in the Indochina Peninsula. We compiled the existing isotope data for Cenozoic basalts in the Indochina Peninsula and adjacent regions (Figures 5 and 9). Basalts in Northern Vietnam (Hoang et al., 1996), Hainan Island (Wang et al., 2013), the EVS/SCS (seamount, Tu et al., 1992; Yan et al., 2008) and Eastern Thailand (e.g., Group II basalts in Khorat Plateau, Zhou & Mukasa, 1997; Yan et al., 2018) show isotopic compositions similar to the Central Group of Vietnamese basalts. Whereas basalts in Western Thailand (e.g., Denchai, Lop Buri, and Chanthaburi-Trat basalts; Mukasa et al., 1996) and Group I basalts in Khorat Plateau (Zhou & Mukasa, 1997) show isotopic compositions similar to the Southern Group of Vietnamese basalts. Compositional heterogeneity is thus considered to be extended to the mantle beneath the entire Indochina Peninsula. Such large-scale isotopic distinction of basalts in the peninsula is interpreted as the surface expression of different mantle domains having been formed in response to deep mantle upwelling (Figure 9).

Subduction of cold oceanic lithosphere is considered to be a major trigger of convection in the hot asthenosphere. Seismic tomography detected high seismic velocity anomalies at depths of *c.* 400–600 km beneath the Indochina Peninsula (Figure 10). Those anomalies are interpreted as stagnant slabs of the Indo-Australian plate subducted from the southwest and the Pacific plate subducted from the east (e.g., Yu Y. et al., 2017a; Zhao et al., 2021). Numerical modeling predicted that bi-vergent subduction of two oceanic lithospheres, mainly consisting of dense mafic rocks, induces the convection cells and vigorous upwelling at their interface (Figure 10b; Lyu et al., 2019). We speculated that this interface could be located in south-central/north-southern Vietnam, consistent with the largest eruption volume in this region among volcanic fields (Figure 10a). The convergent rates of the Indo-Australian plate and the Pacific plate, relative to trenches, are 5–8 cm yr^{-1} (Duarte & Schellart, 2016), and the lengths of subducted oceanic lithospheres of these plates from trenches to Central Vietnam are 2,000–2,500 km, estimated from seismic tomography (Hua et al., 2022). With these variables, we estimate 25–30 Myrs for the transport time of oceanic-lithosphere materials (basaltic crust and sediments) to MTZ. Subsequently, these crustal materials would have been incorporated in the upwelling mantle flows and reached the melting regions beneath Vietnam. Assuming the upwelling velocity of 10–50 km Myr^{-1} for asthenospheric flow (Dasgupta & Mandal, 2022), the storage time of these crustal materials in the mantle is 30–90 Myrs, consistent with the estimates (<100 Myrs) by the forward modeling of the isotope evolution of recycled crustal materials (Y.-Q. Li et al., 2020). We infer that the isotopic features of these isolated domains have been produced by the subduction of crustal materials into the mantle since the late Cretaceous. This inference is supported by the plate reconstruction model; the Indo-Australian and (paleo) Pacific plates have been subducted into the SE Asian mantle since the Cretaceous (insert in Figure 10a; Schellart et al. [2019]).

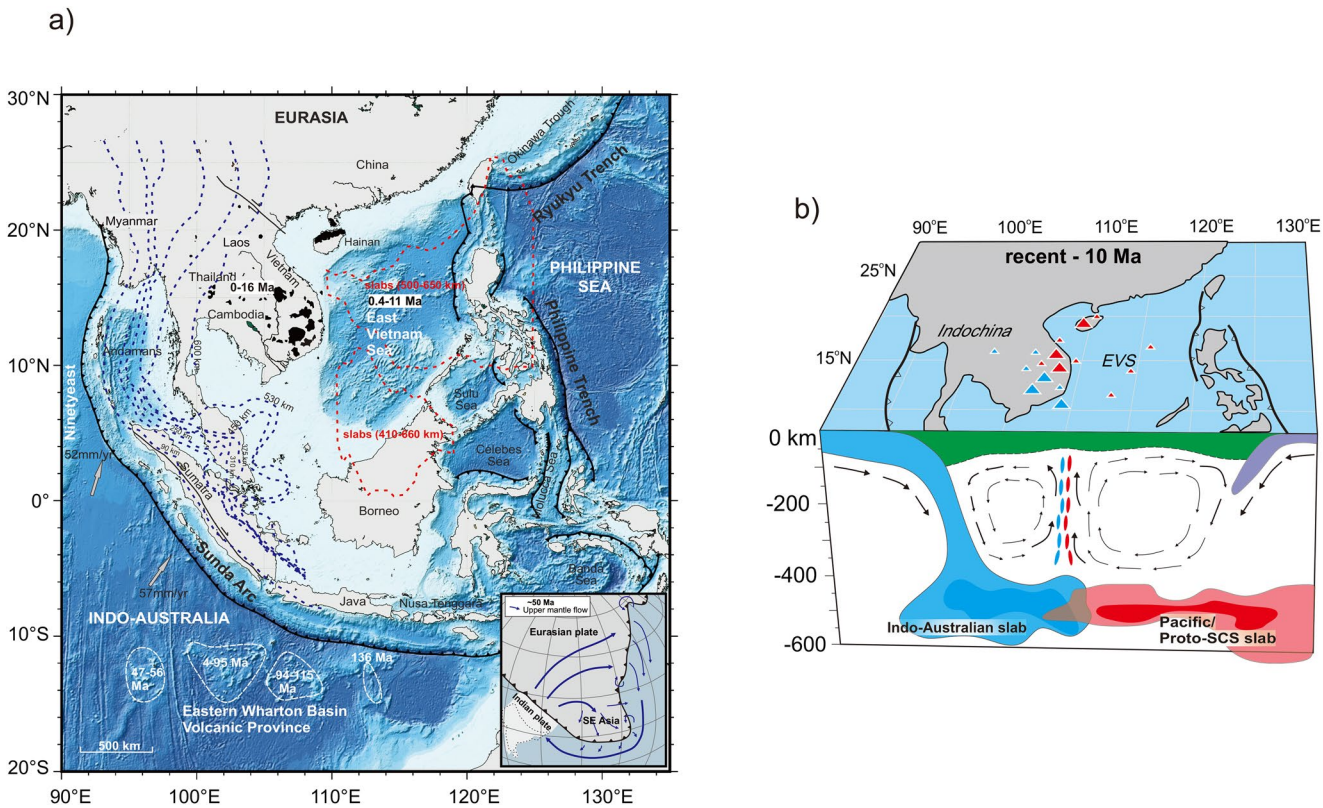

Figure 10. Implication for Cenozoic volcanism in SE Asia. **(a)** Map showing the occurrence of Cenozoic basalts (regions filled by black) in the Indochina Peninsula (16–0 Ma; this study; An et al., 2017; Hoang et al., 2019; Hoàng et al., 2013; Lee et al., 1998; Mukasa et al., 1996; Sieh et al., 2020; Yan et al., 2018) and East Vietnam Sea (11–0.4 Ma; Kudrass et al., 1986; Tu et al., 1992; Yan et al., 2008). The blue dashed lines with numbers indicate the depth contours of the subducted Indo-Australian slab in the mantle (100–600 km, Jacob et al., 2014; Pesicek et al., 2008). The red dashed lines indicate where the Pacific slabs reside at given depths (410–660 or 500–650 km) in western SE Asia (Hua et al., 2022; Wu et al., 2016). An insert shows the simplified tectonic map at *c*. 50 Ma (redraw after Schellart et al., 2019) showing two oceanic plates, the Indo-Australian and Pacific plates, in the southwest and east, respectively, subducted into the SE Asian mantle. **(b)** Cartoon illustrating the formation of isolated, two convecting cells (flow directions are shown by arrows) in asthenosphere, induced by subductions of the Pacific and Indo-Australian plates with inward-dipping (10 Ma to recent). Crustal materials of subducted oceanic lithospheres have been entrained into each convecting cells and transported to melting regions beneath the volcanic fields (blue triangles, volcanic fields largely contributed from the Indo-Australian slab; red triangles, volcanic fields largely contributed from the Pacific slab).

6. Conclusion

The conclusion of this study is summarized as:

1. Intraplate volcanism in SE Asia occurred shortly after cessation of the EVS/SCS and intensively over the last 10 Myrs (peak at 2 Ma) centralized in south-central Vietnam.
2. Magmas erupted in Central and Southern Vietnam have likely been produced at sub-lithospheric depths from sources dominated by ultramafic peridotite with subordinate mafic/ultramafic lithologies.
3. Basalts in Central and Southern Vietnam have statistically different isotopic characteristics, owing to the involvements of different mantle end-member components; EM1-like source in Southern Vietnam and EM2-like source in Central Group basalts, respectively.
4. The Central Group samples are characterized by highly radiogenic Sr-Pb compositions and enrichments of Pb and Th which were likely derived from a source with a contribution of subducted sediment (EM2) that originated from the Pacific slab. Whereas the Southern Group samples are characterized by low $^{143}Nd/^{144}Nd$ and $^{207 \text{ or } 208}Pb/^{204}Pb$, variable $^{206}Pb/^{204}Pb$ and enrichments of Sr and Th. These basalts resemble magmas that tapped an enriched mantle (EM1)-like source, and are interpreted as the contribution of seamount segments from the Indo-Australian oceanic lithosphere.

5. The new model proposed here is that the subduction of two different oceanic lithospheres transfers heterogeneous crustal materials to the deep mantle. Subsequently, dense crustal materials (mafic rocks) induce mantle upwelling which incorporates these and the other crustal materials (sediments) back to shallow depths and trigger intraplate volcanism in SE Asia.
6. We infer that south-central Vietnam is the center of mantle upwelling, where two slabs were interfaced in the mantle, leading to vigorous ascending mantle flows between two convecting cells and resulting in intensive surface volcanism.

Data Availability Statement

The data used in this research are available at the Zenodo open data repository (https://doi.org/10.5281/zenodo.6387524) and are also provided in the Supporting Information S1. Figures 1 and 10 were prepared using GMT (Wessel et al., 2013).

Acknowledgments
The authors are grateful to C. Potiszil, T. Kunihiro, R. Tanaka, T. Ota and H. Tripathi for their constructive discussions. All members of Pheasant Memorial Laboratory are thanked for their technical support and constructive discussions. We thank Lynne Elkins, Associate Editor John Lassiter and an anonymous reviewer for constructive and detailed comments which greatly improved this manuscript, and Stephen Parman for his editorial handling. This study was supported by the MEXT (Ministry of Education, Culture, Sports, Science, and Technology).

References

An, A.-R., Choi, S. H., Yu, Y., & Lee, D.-C. (2017). Petrogenesis of late Cenozoic basaltic rocks from southern Vietnam. *Lithos*, *272–273*, 192–204. https://doi.org/10.1016/j.lithos.2016.12.008

Anh, H. T. H., Choi, S. H., Yu, Y., & Hieu, P. T. (2020). Geochemical constraints on the evolution of the lithospheric mantle beneath central and southern Vietnam. *Geosciences Journal*, *25*, 433–451. https://doi.org/10.1007/s12303-020-0045-4

Baker, J., Peate, D., Waight, T., & Meyzen, C. (2004). Pb isotopic analysis of standards and samples using a ^{207}Pb–^{204}Pb double spike and thallium to correct for mass bias with a double-focusing MC-ICP-MS. *Chemical Geology*, *211*(3), 275–303. https://doi.org/10.1016/j.chemgeo.2004.06.030

Ball, P. W., White, N. J., Maclennan, J., & Stephenson, S. N. (2021). Global influence of mantle temperature and plate thickness on intraplate volcanism. *Nature Communications*, *12*(1), 2045. https://doi.org/10.1038/s41467-021-22323-9

Barr, S., & Macdonald, A. (1981). Geochemistry and geochronology of late Cenozoic basalts of Southeast Asia: Summary. *The Geological Society of America Bulletin*, *92*, 508. https://doi.org/10.1130/0016-7606(1981)92<508:GAGOLC>2.0.CO;2

Ben Othman, D., White, W. M., & Patchett, J. (1989). The geochemistry of marine sediments, island arc magma genesis, and crust-mantle recycling. *Earth and Planetary Science Letters*, *94*(1–2), 1–21. https://doi.org/10.1016/0012-821X(89)90079-4

Blundy, J., Melekhova, E., Ziberna, L., Humphreys, M., Cerantola, V., Brooker, R. A., et al. (2020). Effect of redox on Fe–Mg–Mn exchange between olivine and melt and an oxybarometer for basalts. *Contributions to Mineralogy and Petrology*, *175*(11), 1–32. https://doi.org/10.1007/s00410-020-01736-7

Bohrson, W. A., Spera, F. J., Ghiorso, M. S., Brown, G. A., Creamer, J. B., & Mayfield, A. (2014). Thermodynamic model for energy-constrained open-system evolution of crustal magma bodies undergoing simultaneous recharge, assimilation and crystallization: The magma chamber simulator. *Journal of Petrology*, *55*(9), 1685–1717. https://doi.org/10.1093/petrology/egu036

Bohrson, W. A., Spera, F. J., Heinonen, J. S., Brown, G. A., Scruggs, M. A., Adams, J. V., et al. (2020). Diagnosing open-system magmatic processes using the magma chamber simulator (MCS): Part I—Major elements and phase equilibria. *Contributions to Mineralogy and Petrology*, *175*(11), 104. https://doi.org/10.1007/s00410-020-01722-z

Brown, E. L., & Lesher, C. E. (2016). REEBOX PRO: A forward model simulating melting of thermally and lithologically variable upwelling mantle. *Geochemistry, Geophysics, Geosystems*, *17*(10), 3929–3968. https://doi.org/10.1002/2016GC006579

Choi, S. H., Mukasa, S. B., Zhou, X.-H., Xian, X. H., & Andronikov, A. V. (2008). Mantle dynamics beneath East Asia constrained by Sr, Nd, Pb and Hf isotopic systematics of ultramafic xenoliths and their host basalts from Hannuoba, North China. *Chemical Geology*, *248*(1), 40–61. https://doi.org/10.1016/j.chemgeo.2007.10.008

Clift, P., Lee, G. H., Duc, N. A., Barckhausen, U., Long, H. V., & Zhen, S. (2008). Seismic reflection evidence for a dangerous grounds miniplate: No extrusion origin for the South China Sea. *Tectonics*, *27*(3), TC3008. https://doi.org/10.1029/2007TC002216

Cloos, M. (1993). Lithospheric buoyancy and collisional orogenesis: Subduction of oceanic plateaus, continental margins, island arcs, spreading ridges, and seamounts. *GSA Bulletin*, *105*(6), 715–737. https://doi.org/10.1130/0016-7606(1993)105<0715:LBACOS>2.3.CO;2

Condamine, P., Médard, E., & Devidal, J.-L. (2016). Experimental melting of phlogopite-peridotite in the garnet stability field. *Contributions to Mineralogy and Petrology*, *171*(11), 95. https://doi.org/10.1007/s00410-016-1306-0

Dasgupta, R., Jackson, M. G., & Lee, C.-T. A. (2010). Major element chemistry of ocean island basalts — conditions of mantle melting and heterogeneity of mantle source. *Earth and Planetary Science Letters*, *289*(3), 377–392. https://doi.org/10.1016/j.epsl.2009.11.027

Dasgupta, R., Mallik, A., Tsuno, K., Withers, A. C., Hirth, G., & Hirschmann, M. M. (2013). Carbon-dioxide-rich silicate melt in the Earth's upper mantle. *Nature*, *493*(7431), 211–215. https://doi.org/10.1038/nature11731

Dasgupta, R., & Mandal, N. (2022). Role of double-subduction dynamics in the topographic evolution of the Sunda plate. *Geophysical Journal International*, *230*, 696–713. *ggac025*. https://doi.org/10.1093/gji/ggac025

Davis, F. A., & Hirschmann, M. M. (2013). The effects of K_2O on the compositions of near-solidus melts of garnet peridotite at 3 GPa and the origin of basalts from enriched mantle. *Contributions to Mineralogy and Petrology*, *166*(4), 1029–1046. https://doi.org/10.1007/s00410-013-0907-0

Davis, F. A., Hirschmann, M. M., & Humayun, M. (2011). The composition of the incipient partial melt of garnet peridotite at 3 GPa and the origin of OIB. *Earth and Planetary Science Letters*, *308*(3), 380–390. https://doi.org/10.1016/j.epsl.2011.06.008

Dixon, J. E., Clague, D. A., Wallace, P., & Poreda, R. (1997). Volatiles in alkalic basalts form the North Arch Volcanic Field, Hawaii: Extensive degassing of deep submarine-erupted alkalic series lavas. *Journal of Petrology*, *38*(7), 911–939. https://doi.org/10.1093/petroj/38.7.911

Dixon, J. E., Leist, L., Langmuir, C., & Schilling, J.-G. (2002). Recycled dehydrated lithosphere observed in plume-influenced mid-ocean-ridge basalt. *Nature*, *420*(6914), 385–389. https://doi.org/10.1038/nature01215

Duarte, J., & Schellart, W. (2016). *Introduction to plate boundaries and natural hazards*. In J. C. Duarte, & W. P. Schellart (Eds.), *Plate Boundaries and Natural Hazards, Geophysical Monograph* (Vol. 219, pp. 1–10). Wiley Online Library. https://doi.org/10.1002/9781119054146.ch1

Falloon, T. J., & Danyushevsky, L. V. (2000). Melting of Refractory Mantle at 1.5, 2 and 2.5 GPa under anhydrous and H_2O-undersaturated conditions: Implications for the petrogenesis of high-Ca Boninites and the influence of subduction components on mantle melting. *Journal of Petrology*, *41*(2), 257–283. https://doi.org/10.1093/petrology/41.2.257

Fan, J., & Zhao, D. (2019). P-wave anisotropic tomography of the central and southern Philippines. *Physics of the Earth and Planetary Interiors*, *286*, 154–164. https://doi.org/10.1016/j.pepi.2018.12.001

Feig, S. T., Koepke, J., & Snow, J. E. (2006). Effect of water on tholeiitic basalt phase equilibria: An experimental study under oxidizing conditions. *Contributions to Mineralogy and Petrology*, *152*(5), 611–638. https://doi.org/10.1007/s00410-006-0123-2

Flower, M. F. J., Zhang, M., Chen, C.-Y., Tu, K., & Xie, G. (1992). Magmatism in the South China Basin: 2. Post-spreading Quaternary basalts from Hainan island, south China. *Chemical Geology*, *97*(1), 65–87. https://doi.org/10.1016/0009-2541(92)90136-S

Flower, M. F. J., Russo, R. M., Tamaki, K., & Hoang, N. (2001). Mantle contamination and the Izu-Bonin-Mariana (IBM) 'high-tide mark': Evidence for mantle extrusion caused by Tethyan closure. *Tectonophysics*, *333*, 9–34. https://doi.org/10.1016/S0040-1951(00)00264-X

Flower, M., Tamaki, K., & Hoang, N. (1998). *Mantle extrusion: A model for dispersed volcanism and DUPAL-like asthenosphere in East Asia and the Western Pacific*. In M. J. Flower, S.-L. Chung, C.-H. Lo, & T.-Y. Lee (Eds.), *Mantle Dynamics and Plate Interactions in East Asia, Geodynamic Series*. (Vol. 27, pp. 67–88). Wiley Online Library. https://doi.org/10.1029/GD027p0067

Fukao, Y., & Obayashi, M. (2013). Subducted slabs stagnant above, penetrating through, and trapped below the 660 km discontinuity. *Journal of Geophysical Research: Solid Earth*, *118*(11), 5920–5938. https://doi.org/10.1002/2013JB010466

Gale, A., Dalton, C. A., Langmuir, C. H., Su, Y., & Schilling, J.-G. (2013). The mean composition of ocean ridge basalts. *Geochemistry, Geophysics, Geosystems*, *14*(3), 489–518. https://doi.org/10.1029/2012GC004334

Gasparon, M., & Varne, R. (1998). Crustal assimilation versus subducted sediment input in west Sunda arc volcanics: An evaluation. *Mineralogy and Petrology*, *64*(1–4), 89–117. https://doi.org/10.1007/BF01226565

Gasperini, D., Blichert-Toft, J., Bosch, D., Moro, A. D., Macera, P., Télouk, P., & Albarède, F. (2000). Evidence from Sardinian basalt geochemistry for recycling of plume heads into the Earth's mantle. *Nature*, *408*(6813), 701–704. https://doi.org/10.1038/35047049

Gavrilenko, M., Herzberg, C., Vidito, C., Carr, M. J., Tenner, T., & Ozerov, A. (2016). A calcium-in-olivine geohygrometer and its application to subduction zone magmatism. *Journal of Petrology*, *57*(9), 1811–1832. https://doi.org/10.1093/petrology/egw062

Gleeson, M. L. M., & Gibson, S. A. (2019). Crustal controls on apparent mantle pyroxenite signals in ocean-island basalts. *Geology*, *47*(4), 321–324. https://doi.org/10.1130/G45759.1

Green, D. H. (1973). Experimental melting studies on a model upper mantle composition at high pressure under water-saturated and water-undersaturated conditions. *Earth and Planetary Science Letters*, *19*(1), 37–53. https://doi.org/10.1016/0012-821X(73)90176-3

Hall, R. (2002). Cenozoic geological and plate tectonic evolution of SE Asia and the SW Pacific: Computer-based reconstructions, model and animations. *Journal of Asian Earth Sciences*, *20*(4), 353–431. https://doi.org/10.1016/S1367-9120(01)00069-4

Hart, S. R. (1984). A large-scale isotope anomaly in the Southern Hemisphere mantle. *Nature*, *309*(5971), 753–757. https://doi.org/10.1038/309753a0

Heinonen, J. S., Bohrson, W. A., Spera, F. J., Brown, G. A., Scruggs, M. A., & Adams, J. V. (2020). Diagnosing open-system magmatic processes using the magma Chamber simulator (MCS): Part II—Trace elements and isotopes. *Contributions to Mineralogy and Petrology*, *175*(11), 105. https://doi.org/10.1007/s00410-020-01718-9

Herzberg, C., & Asimow, P. D. (2015). PRIMELT3 MEGA.XLSM software for primary magma calculation: Peridotite primary magma MgO contents from the liquidus to the solidus. *Geochemistry, Geophysics, Geosystems*, *16*(2), 563–578. https://doi.org/10.1002/2014GC005631

Hirose, K. (1997). Partial melt compositions of carbonated peridotite at 3 GPa and role of CO_2 in alkali-basalt magma generation. *Geophysical Research Letters*, *24*(22), 2837–2840. https://doi.org/10.1029/97GL02956

Hirose, K., & Kawamura, K. (1994). A new experimental approach for incremental batch melting of peridotite at 1.5 GPa. *Geophysical Research Letters*, *21*(19), 2139–2142. https://doi.org/10.1029/94GL01792

Hirose, K., & Kushiro, I. (1993). Partial melting of dry peridotites at high pressures: Determination of compositions of melts segregated from peridotite using aggregates of diamond. *Earth and Planetary Science Letters*, *114*(4), 477–489. https://doi.org/10.1016/0012-821X(93)90077-M

Hirose, K., & Kushiro, I. (1998). The effect of melt segregation on polybaric mantle melting: Estimation from the incremental melting experiments. *Physics of the Earth and Planetary Interiors*, *107*(1), 111–118. https://doi.org/10.1016/S0031-9201(97)00129-5

Hirschmann, M. M. (2000). Mantle solidus: Experimental constraints and the effects of peridotite composition. *Geochemistry, Geophysics, Geosystems*, *1*(10), 1042. https://doi.org/10.1029/2000GC000070

Hirschmann, M. M. (2006). Water, melting, and the deep Earth H_2O cycle. *Annual Review of Earth and Planetary Sciences*, *34*(1), 629–653. https://doi.org/10.1146/annurev.earth.34.031405.125211

Hirschmann, M. M., Kogiso, T., Baker, M. B., & Stolper, E. M. (2003). Alkalic magmas generated by partial melting of garnet pyroxenite. *Geology*, *31*(6), 481–484. https://doi.org/10.1130/0091-7613(2003)031<0481:AMGBPM>2.0.CO;2

Hoang, N., & Flower, M. (1998). Petrogenesis of Cenozoic basalts from Vietnam: Implication for origins of a 'diffuse igneous province. *Journal of Petrology*, *39*(3), 369–395. https://doi.org/10.1093/petroj/39.3.369

Hoang, N., Flower, M. F. J., & Carlson, R. W. (1996). Major, trace element, and isotopic compositions of Vietnamese basalts: Interaction of hydrous EM1-rich asthenosphere with thinned Eurasian lithosphere. *Geochimica et Cosmochimica Acta*, *60*(22), 4329–4351. https://doi.org/10.1016/S0016-7037(96)00247-5

Hoàng, N., Flower, M. F. J., Chí, C. T., Xuân, P. T., Quý, H. V., & Sơn, T. T. (2013). Collision-induced basalt eruptions at Pleiku and Buôn Mê Thuột, south-central Viet Nam. *Journal of Geodynamics*, *69*, 65–83. https://doi.org/10.1016/j.jog.2012.03.012

Hoang, N., Shinjo, R., Phuc, L. T., Anh, L. D., Huong, T. T., Pécskay, Z., & Bac, D. T. (2019). Pleistocene basaltic volcanism in the Krông Nô area and vicinity, Dac Nong Province (Vietnam). *Journal of Asian Earth Sciences*, *181*, 103903. https://doi.org/10.1016/j.jseaes.2019.103903

Hoang, T. H. A., Choi, S. H., Yu, Y., Pham, T. H., Nguyen, K. H., & Ryu, J.-S. (2018). Geochemical constraints on the spatial distribution of recycled oceanic crust in the mantle source of late Cenozoic basalts, Vietnam. *Lithos*, *296–299*, 382–395. https://doi.org/10.1016/j.lithos.2017.11.020

Ho, K., Chen, J., & Juang, W. (2000). Geochronology and geochemistry of late Cenozoic basalts from the Leiqiong area, southern China. *Journal of Asian Earth Sciences*, *18*(3), 307–324. https://doi.org/10.1016/S1367-9120(99)00059-0

Hoernle, K., Hauff, F., Werner, R., van den Bogaard, P., Gibbons, A. D., Conrad, S., & Müller, R. D. (2011). Origin of Indian Ocean Seamount Province by shallow recycling of continental lithosphere. *Nature Geoscience*, *4*(12), 883–887. https://doi.org/10.1038/ngeo1331

Huang, Z., Zhao, D., & Wang, L. (2015). P wave tomography and anisotropy beneath Southeast Asia: Insight into mantle dynamics. *Journal of Geophysical Research: Solid Earth*, *120*(7), 5154–5174. https://doi.org/10.1002/2015JB012098

Hua, Y., Zhao, D., & Xu, Y.-G. (2022). Azimuthal anisotropy tomography of the Southeast Asia subduction system. *Journal of Geophysical Research: Solid Earth*, *127*, e2021JB022854. https://doi.org/10.1029/2021JB022854

Huong, T. T., & Hoang, N. (2018). Petrology, geochemistry, and Sr, Nd isotopes of mantle xenolith in Nghia Dan alkaline basalt (West Nghe An): Implications for lithospheric mantle characteristics beneath the region. *Vietnam Journal of Earth Sciences*, *40*(3), 207–227. https://doi.org/10.15625/0866-7187/40/3/12614

Irifune, T., Ringwood, A. E., & Hibberson, W. O. (1994). Subduction of continental crust and terrigenous and pelagic sediments: An experimental study. *Earth and Planetary Science Letters*, *126*(4), 351–368. https://doi.org/10.1016/0012-821X(94)90117-1

Irvine, T. N. J., & Baragar, W. R. A. (1971). A guide to the chemical classification of the common volcanic rocks. *Canadian Journal of Earth Sciences*, *8*(5), 523–548. https://doi.org/10.1139/e71-055

Jacob, J., Dyment, J., & Yatheesh, V. (2014). Revisiting the structure, age, and evolution of the Wharton Basin to better understand subduction under Indonesia. *Journal of Geophysical Research: Solid Earth*, *119*(1), 169–190. https://doi.org/10.1002/2013JB010285

Jiang, W., Yu, J. H., Wang, X., Griffin, W. L., Pham, T., Nguyen, D., & Wang, F. (2020). Early Paleozoic magmatism in northern Kontum massif, central Vietnam: Insights into tectonic evolution of the eastern Indochina block. *Lithos*, *376–377*, 105750. https://doi.org/10.1016/j.lithos.2020.105750

Katz, R. F., Spiegelman, M., & Langmuir, C. H. (2003). A new parameterization of hydrous mantle melting. *Geochemistry, Geophysics, Geosystems*, *4*(9), 1073. https://doi.org/10.1029/2002GC000433

Kelley, K. A., & Cottrell, E. (2009). Water and the oxidation state of subduction zone magmas. *Science*, *325*(5940), 605–607. https://doi.org/10.1126/science.1174156

Kogiso, T., Hirschmann, M. M., & Frost, D. J. (2003). High-pressure partial melting of garnet pyroxenite: Possible mafic lithologies in the source of ocean island basalts. *Earth and Planetary Science Letters*, *216*(4), 603–617. https://doi.org/10.1016/S0012-821X(03)00538-7

Koszowska, E., Wolska, A., Zuchiewicz, W., Cuong, N. Q., & Pécskay, Z. (2007). Crustal contamination of late Neogene basalts in the Dien Bien Phu basin, NW Vietnam: Some insights from petrological and geochronological studies. *Journal of Asian Earth Sciences*, *29*(1), 1–17. https://doi.org/10.1016/j.jseaes.2005.12.003

Kudrass, H. R., Wiedicke, M., Cepek, P., Kreuzer, H., & Müller, P. (1986). Mesozoic and Cainozoic rocks dredged from the South China Sea (Reed Bank area) and Sulu Sea and their significance for plate-tectonic reconstructions. *Marine and Petroleum Geology*, *3*(1), 19–30. https://doi.org/10.1016/0264-8172(86)90053-X

Kuritani, T., & Nakamura, E. (2002). Precise isotope analysis of nanogram-level Pb for natural rock samples without use of double spikes. *Chemical Geology*, *186*(1–2), 31–43. https://doi.org/10.1016/s0009-2541(02)00004-9

Kuritani, T., & Nakamura, E. (2003). Highly precise and accurate isotopic analysis of small amounts of Pb using ^{205}Pb–^{204}Pb and ^{207}Pb-^{204}Pb, two double spikes. *Journal of Analytical Atomic Spectrometry*, *18*(12), 1464–1470. https://doi.org/10.1039/B310294G

Kuritani, T., Ohtani, E., & Kimura, J.-I. (2011). Intensive hydration of the mantle transition zone beneath China caused by ancient slab stagnation. *Nature Geoscience*, *4*(10), 713–716. https://doi.org/10.1038/ngeo1250

Kushiro, I. (1996). *Partial melting of fertile mantle peridotite at high pressures: An experimental study using aggregates of diamond*. In A. Basu, & S. Hart (Eds.), *Earth Processes: Reading the Isotopic Code, Geophysical Monograph*. (Vol. 95, pp. 109–122). Wiley Online Library. https://doi.org/10.1029/GM095p0109

Lan, C. Y., Chung, S. L., Van Long, T., Lo, C. H., Lee, T. Y., Mertzman, S. A., & Shen, J. J.-S. (2003). Geochemical and Sr–Nd isotopic constraints from the Kontum massif, central Vietnam on the crustal evolution of the Indochina block. *Precambrian Research*, *122*(1–4), 7–27. https://doi.org/10.1016/S0301-9268(02)00205-X

Langmuir, C. H., Klein, E. M., & Plank, T. (1992). *Petrological systematics of mid-ocean ridge basalts: Constraints on melt generation beneath ocean ridges*. In J. P. Morgan, D. K. Blackman, & J. M. Sinton (Eds.), *Mantle Flow and Melt Generation at Mid-Ocean Ridges, Geophysical Monograph* (Vol. 71, pp. 183–280). Wiley Online Library. https://doi.org/10.1029/GM071p0183

Lee, C.-T. A., Luffi, P., Plank, T., Dalton, H., & Leeman, W. P. (2009). Constraints on the depths and temperatures of basaltic magma generation on Earth and other terrestrial planets using new thermobarometers for mafic magmas. *Earth and Planetary Science Letters*, *279*(1), 20–33. https://doi.org/10.1016/j.epsl.2008.12.020

Lee, T., Lo, C.-H., Chung, S.-L., Chen, C.-Y., Wang, P.-L., Lin, W.-P., et al. (1998). *^{40}Ar/^{39}Ar dating result of Neogene basalts in Vietnam and its tectonic implication*. In M. J. Flower, S.-L. Chung, C.-H. Lo, & T.-Y. Lee (Eds.), *Mantle Dynamics and Plate Interactions in East Asia, Geodynamic Series* (Vol. 27, pp. 317–330). Wiley Online Library. https://doi.org/10.1029/GD027p0317

Le, D. A., Nguyen, H., Phung, V. P., Dinh, Q. S., & Shakirov, R. (2019). Geochemical features of olivines from Northeastern Phu Quy Volcanic Island and their relation to melt variations in the magma source. *Series B*, 49–50.

Li, C.-F., Xu, X., Lin, J., Sun, Z., Zhu, J., Yao, Y., et al. (2014). Ages and magnetic structures of the South China Sea constrained by deep tow magnetic surveys and IODP Expedition 349. *Geochemistry, Geophysics, Geosystems*, *15*(12), 4958–4983. https://doi.org/10.1002/2014GC005567

Li, Y.-Q., Kitagawa, H., Nakamura, E., Ma, C., Hu, X., Kobayashi, K., & Sakaguchi, C. (2020). Various ages of recycled material in the source of Cenozoic basalts in SE China: Implications for the role of the Hainan Plume. *Journal of Petrology*, *61*(6), egaa060. https://doi.org/10.1093/petrology/egaa060

Liu, J.-Q., Ren, Z.-Y., Nichols, A. R. L., Song, M.-S., Qian, S.-P., Zhang, Y., & Zhao, P.-P. (2015). Petrogenesis of late Cenozoic basalts from north Hainan island: Constraints from melt inclusions and their host olivines. *Geochimica et Cosmochimica Acta*, *152*, 89–121. https://doi.org/10.1016/j.gca.2014.12.023

Lu, Y., Makishima, A., & Nakamura, E. (2007). Coprecipitation of Ti, Mo, Sn and Sb with fluorides and application to determination of B, Ti, Zr, Nb, Mo, Sn, Sb, Hf and Ta by ICP-MS. *Chemical Geology*, *236*(1–2), 13–26. https://doi.org/10.1016/j.chemgeo.2006.08.007

Lyu, T., Zhu, Z., & Wu, B. (2019). Subducting slab morphology and mantle transition zone upwelling in double-slab subduction models with inward-dipping directions. *Geophysical Journal International*, *218*(3), 2089–2105. https://doi.org/10.1093/gji/ggz268

Makishima, A., & Nakamura, E. (2006). Determination of major/minor and trace elements in silicate samples by ICP-QMS and ICP-SFMS applying isotope dilution-internal standardisation (ID-IS) and multi-stage internal standardisation. *Geostandards and Geoanalytical Research*, *30*(3), 245–271. https://doi.org/10.1111/j.1751-908X.2006.tb01066.x

Mather, B. R., Müller, R. D., Seton, M., Ruttor, S., Nebel, O., & Mortimer, N. (2020). Intraplate volcanism triggered by bursts in slab flux. *Science Advances*, *6*(51), eabd0953. https://doi.org/10.1126/sciadv.abd0953

Matzen, A. K., Wood, B. J., Baker, M. B., & Stolper, E. M. (2017). The roles of pyroxenite and peridotite in the mantle sources of oceanic basalts. *Nature Geoscience*, *10*(7), 530–535. https://doi.org/10.1038/ngeo2968

McDonough, W. F., & Sun, S.-s. (1995). The composition of the Earth. *Chemical Geology*, *120*(3–4), 223–253. https://doi.org/10.1016/0009-2541(94)00140-4

Metcalfe, I. (2013). Asia; south-east. In S. A. Elias (Ed.), *Reference Module in earth systems and Environmental Sciences*. Elsevier. https://doi.org/10.1016/B978-0-12-409548-9.02721-4

Montelli, R., Nolet, G., Dahlen, F. A., & Masters, G. (2006). A catalogue of deep mantle plumes: New results from finite-frequency tomography. *Geochemistry, Geophysics, Geosystems*, *7*(11), Q11007. https://doi.org/10.1029/2006GC001248

Mukasa, S. B., Fischer, G. M., & Barr, S. M. (1996). The character of the subcontinental mantle in Southeast Asia: Evidence from isotopic and elemental compositions of extension-related Cenozoic basalts in Thailand. In A. Basu, & S. Hart (Eds.), *Earth Processes: Reading the Isotopic Code Earth Processes, Geophysical Monograph* (Vol. 95, pp. 233–252). https://doi.org/10.1029/GM095p0233

Murphy, D. T., Collerson, K. D., & Kamber, B. S. (2002). Lamproites from Gaussberg, Antarctica: Possible transition zone melts of Archaean subducted sediments. *Journal of Petrology*, *43*(6), 981–1001. https://doi.org/10.1093/petrology/43.6.981

Nakamura, E., Campbell, I. H., & Sun, S.-s. (1985). The influence of subduction processes on the geochemistry of Japanese alkaline basalts. *Nature*, *316*(6023), 55–58. https://doi.org/10.1038/316055a0

Nakamura, E., Makishima, A., Moriguti, T., Kobayashi, K., Sakaguchi, C., Yokoyama, T., et al. (2003). *Comprehensive geochemical analyses of small amounts (~100 mg) of extraterrestrial samples for the analytical competition related to the sample return mission MUSES-C. The Institute of Space and Astronautical Science Report*. (Vol. 16, pp. 49–101).

Nakamura, E., McDougall, I., & Campbell, I. H. (1986). K-Ar ages of basalts from the Higashi-Matsuura district, northwestern Kyushu, Japan and regional geochronology of the Cenozoic alkaline volcanic rocks in eastern Asia. *Geochemical Journal*, *20*(2), 91–99. https://doi.org/10.2343/geochemj.20.91

Nguyen, C., & Kil, Y. (2020). Petrological characteristics of lithospheric mantle beneath Nui Nua and Ba Ria areas, southern Vietnam. *Geosciences Journal*, *24*(5), 475–487. https://doi.org/10.1007/s12303-020-0017-8

Nguyen, T. T., Kitagawa, H., Pineda-Velasco, I., & Nakamura, E. (2020). Feedback of slab distortion on volcanic arc evolution: Geochemical perspective from late Cenozoic volcanism in SW Japan. *Journal of Geophysical Research: Solid Earth*, *125*(10), e2019JB019143. https://doi.org/10.1029/2019JB019143

Nguyen, T. T. B., Satir, M., Siebel, W., & Chen, F. (2004). Granitoids in the Dalat zone, southern Vietnam: Age constraints on magmatism and regional geological implications. *International Journal of Earth Sciences*, *93*(3), 329–340. https://doi.org/10.1007/s00531-004-0387-6

Nguyen, T. T. B., Satir, M., Siebel, W., Vennemann, T., & Van Long, T. (2004). Geochemical and isotopic constraints on the petrogenesis of granitoids from the Dalat zone, southern Vietnam. *Journal of Asian Earth Sciences*, *23*(4), 467–482. https://doi.org/10.1016/j.jseaes.2003.06.001

Owada, M., Osanai, Y., Nakano, N., Matsushita, T., Tran Ngoc Nam, Tsunogae, T., Tsunogae, T., et al. (2007). Crustal anatexis and formation of two types of granitic magmas in the Kontum massif, central Vietnam: Implications for magma processes in collision zones. *Gondwana Research*, *12*(4), 428–437. https://doi.org/10.1016/j.gr.2006.11.001

Pesicek, J. D., Thurber, C. H., Widiyantoro, S., Engdahl, E. R., & DeShon, H. R. (2008). Complex slab subduction beneath northern Sumatra. *Geophysical Research Letters*, *35*(20), L20303. https://doi.org/10.1029/2008GL035262

Pickering-Witter, J., & Johnston, A. D. (2000). The effects of variable bulk composition on the melting systematics of fertile peridotitic assemblages. *Contributions to Mineralogy and Petrology*, *140*(2), 190–211. https://doi.org/10.1007/s004100000183

Pineda-Velasco, I., Nguyen, T. T., Kitagawa, H., & Nakamura, E. (2015). Comment on "Diverse magmatic effects of subducting a hot slab in SW Japan: Results from forward modeling" by J.-I. Kimura et al. *Geochemistry, Geophysics, Geosystems*, *16*, 2848–2852. https://doi.org/10.1002/2015GC005914

Plank, T. (2005). Constraints from thorium/lanthanum on sediment recycling at subduction zones and the evolution of the continents. *Journal of Petrology*, *46*(5), 921–944. https://doi.org/10.1093/petrology/egi005

Plank, T., & Forsyth, D. W. (2016). Thermal structure and melting conditions in the mantle beneath the Basin and Range province from seismology and petrology. *Geochemistry, Geophysics, Geosystems*, *17*(4), 1312–1338. https://doi.org/10.1002/2015GC006205

Plank, T., & Langmuir, C. H. (1998). The chemical composition of subducting sediment and its consequences for the crust and mantle. *Chemical Geology*, *145*(3–4), 325–394. https://doi.org/10.1016/S0009-2541(97)00150-2

Putirka, K. D. (2008). Thermometers and barometers for volcanic systems. *Reviews in Mineralogy and Geochemistry*, *69*(1), 61–120. https://doi.org/10.2138/rmg.2008.69.3

Putirka, K. (2016). Rates and styles of planetary cooling on Earth, Moon, Mars, and Vesta, using new models for oxygen fugacity, ferric-ferrous ratios, olivine-liquid Fe-Mg exchange, and mantle potential temperature. *American Mineralogist*, *101*(4), 819–840. https://doi.org/10.2138/am-2016-5402

Qian, S., Gazel, E., Nichols, A. R. L., Cheng, H., Zhang, L., Salters, V. J., et al. (2021). The origin of late Cenozoic magmatism in the South China Sea and Southeast Asia. *Geochemistry, Geophysics, Geosystems*, *22*, e2021GC009686. https://doi.org/10.1029/2021GC009686

Rangin, C., Huchon, P., Le Pichon, X., Bellon, H., Lepvrier, C., Roques, D., et al. (1995). Cenozoic deformation of central and south Vietnam. *Tectonophysics*, *251*(1–4), 179–196. https://doi.org/10.1016/0040-1951(95)00006-2

Roeder, P. L., & Emslie, R. F. (1970). Olivine-liquid equilibrium. *Contributions to Mineralogy and Petrology*, *29*(4), 275–289. https://doi.org/10.1007/BF00371276

Sakuyama, T., Tian, W., Kimura, J.-I., Fukao, Y., Hirahara, Y., Takahashi, T., et al. (2013). Melting of dehydrated oceanic crust from the stagnant slab and of the hydrated mantle transition zone: Constraints from Cenozoic alkaline basalts in eastern China. *Chemical Geology*, *359*, 32–48. https://doi.org/10.1016/j.chemgeo.2013.09.012

Salters, V. J. M., & Stracke, A. (2004). Composition of the depleted mantle. *Geochemistry, Geophysics, Geosystems*, *5*(5), Q05B07. https://doi.org/10.1029/2003GC000597

Sarafian, E., Gaetani, G. A., Hauri, E. H., & Sarafian, A. R. (2017). Experimental constraints on the damp peridotite solidus and oceanic mantle potential temperature. *Science*, *355*(6328), 942–945. https://doi.org/10.1126/science.aaj2165

Sawyer, E. W., Cesare, B., & Brown, M. (2011). When the continental crust melts. *Elements*, *7*(4), 229–234. https://doi.org/10.2113/gselements.7.4.229

Schellart, W. P., Chen, Z., Strak, V., Duarte, J. C., & Rosas, F. M. (2019). Pacific subduction control on Asian continental deformation including Tibetan extension and eastward extrusion tectonics. *Nature Communications*, *10*(1), 4480. https://doi.org/10.1038/s41467-019-12337-9

Shellnutt, J. G., Lan, C.-Y., Van Long, T., Usuki, T., Yang, H.-J., Mertzman, S. A., et al. (2013). Formation of Cretaceous Cordilleran and post-orogenic granites and their microgranular enclaves from the Dalat zone, southern Vietnam: Tectonic implications for the evolution of Southeast Asia. *Lithos*, *182–183*, 229–241. https://doi.org/10.1016/j.lithos.2013.09.016

Sieh, K., Herrin, J., Jicha, B., Schonwalder Angel, D., Moore, J. D. P., Banerjee, P., et al. (2020). Australasian impact crater buried under the Bolaven volcanic field, Southern Laos. *Proceedings of the National Academy of Sciences*, *117*(3), 1346–1353. https://doi.org/10.1073/pnas.1904368116

Sobolev, A. V., Hofmann, A. W., Kuzmin, D. V., Yaxley, G. M., Arndt, N. T., Chung, S.-L., et al. (2007). The amount of recycled crust in sources of mantle-derived melts. *Science*, *316*(5823), 412–417. https://doi.org/10.1126/science.1138113

Sobolev, A. V., Hofmann, A. W., & Nikogosian, I. K. (2000). Recycled oceanic crust observed in 'ghost plagioclase' within the source of Mauna Loa lavas. *Nature*, *404*(6781), 986–990. https://doi.org/10.1038/35010098

Sobolev, A. V., Hofmann, A. W., Sobolev, S. V., & Nikogosian, I. K. (2005). An olivine-free mantle source of Hawaiian shield basalts. *Nature*, *434*(7033), 590–597. https://doi.org/10.1038/nature03411

Stracke, A., Bizimis, M., & Salters, V. J. M. (2003). Recycling oceanic crust: Quantitative constraints. *Geochemistry, Geophysics, Geosystems*, *4*(3), 8003. https://doi.org/10.1029/2001GC000223

Stracke, A., Hofmann, A. W., & Hart, S. R. (2005). FOZO, HIMU, and the rest of the mantle zoo. *Geochemistry, Geophysics, Geosystems*, *6*(5), Q05007. https://doi.org/10.1029/2004GC000824

Sun, S.-s., & McDonough, W. F. (1989). Chemical and isotopic systematics of oceanic basalts: Implications for mantle composition and processes. In A. D. Saunders, & M. J. Norry (Eds.), *Magmatism in the Ocean Basins*. (Vol. 42, pp. 313–345). Geological Society, London, Special Publications. https://doi.org/10.1144/GSL.SP.1989.042.01.19

Tanaka, R., Makishima, A., Kitagawa, H., & Nakamura, E. (2003). Suppression of Zr, Nb, Hf and Ta coprecipitation in fluoride compounds for determination in Ca-rich materials. *Journal of Analytical Atomic Spectrometry*, *18*(12), 1458–1463. https://doi.org/10.1039/B309948B

Thirlwall, M. F. (2000). Inter-laboratory and other errors in Pb isotope analyses investigated using a ^{207}Pb–^{204}Pb double spike. *Chemical Geology*, *163*(1), 299–322. https://doi.org/10.1016/S0009-2541(99)00135-7

Tu, K., Flower, M. F. J., Carlson, R. W., Xie, G., Chen, C.-Y., & Zhang, M. (1992). Magmatism in the south China basin: 1. Isotopic and trace-element evidence for an endogenous dupal mantle component. *Chemical Geology*, *97*(1), 47–63. https://doi.org/10.1016/0009-2541(92)90135-R

Walter, M. J. (1998). Melting of garnet peridotite and the origin of komatiite and depleted lithosphere. *Journal of Petrology*, *39*(1), 29–60. https://doi.org/10.1093/petroj/39.1.29

Wang, X.-C., Li, Z.-X., Li, X.-H., Li, J., Liu, Y., Long, W.-G., et al. (2012). Temperature, pressure, and composition of the mantle source region of late Cenozoic basalts in Hainan island, SE Asia: A consequence of a young thermal mantle plume close to subduction zones? *Journal of Petrology*, *53*(1), 177–233. https://doi.org/10.1093/petrology/egr061

Wang, X.-C., Li, Z.-X., Li, X.-H., Li, J., Xu, Y.-G., & Li, X.-H. (2013). Identification of an ancient mantle reservoir and young recycled materials in the source region of a young mantle plume: Implications for potential linkages between plume and plate tectonics. *Earth and Planetary Science Letters*, *377–378*, 248–259. https://doi.org/10.1016/j.epsl.2013.07.003

Wessel, P., Smith, W. H. F., Scharroo, R., Luis, J., & Wobbe, F. (2013). Generic Mapping Tools: Improved Version Released. *Eos, Transactions American Geophysical Union*, *94*(45), 409–410. https://doi.org/10.1002/2013eo450001

Workman, R. K., & Hart, S. R. (2005). Major and trace element composition of the depleted MORB mantle (DMM). *Earth and Planetary Science Letters*, *231*(1), 53–72. https://doi.org/10.1016/j.epsl.2004.12.005

Wu, J., Suppe, J., Lu, R., & Kanda, R. (2016). Philippine Sea and East Asian plate tectonics since 52 Ma constrained by new subducted slab reconstruction methods. *Journal of Geophysical Research: Solid Earth*, *121*(6), 4670–4741. https://doi.org/10.1002/2016JB012923

Yan, Q., Castillo, P., Shi, X., Wang, L., Liao, L., & Ren, J. (2015). Geochemistry and petrogenesis of volcanic rocks from Daimao Seamount (South China Sea) and their tectonic implications. *Lithos*, *218–219*, 117–126. https://doi.org/10.1016/j.lithos.2014.12.023

Yan, Q., Shi, X., Metcalfe, I., Liu, S., Xu, T., Kornkanitnan, N., et al. (2018). Hainan mantle plume produced late Cenozoic basaltic rocks in Thailand, Southeast Asia. *Scientific Reports*, *8*(1), 2640. https://doi.org/10.1038/s41598-018-20712-7

Yan, Q., Shi, X., Wang, K., Bu, W., & Xiao, L. (2008). Major element, trace element, and Sr, Nd and Pb isotope studies of Cenozoic basalts from the South China Sea. *Science in China - Series D: Earth Sciences*, *51*, 550–566. https://doi.org/10.1007/s11430-008-0026-3

Yang, Z.-F., Li, J., Jiang, Q.-B., Xu, F., Guo, S.-Y., Li, Y., & Zhang, J. (2019). Using major element logratios to recognize compositional patterns of basalt: Implications for source lithological and compositional heterogeneities. *Journal of Geophysical Research: Solid Earth*, *124*(4), 3458–3490. https://doi.org/10.1029/2018JB016145

Yokoyama, T., Makishima, A., & Nakamura, E. (1999). Evaluation of the coprecipitation of incompatible trace elements with fluoride during silicate rock dissolution by acid digestion. *Chemical Geology*, *157*(3–4), 175–187. https://doi.org/10.1016/S0009-2541(98)00206-X

Yoshikawa, M., & Nakamura, E. (1993). Precise isotope determination of trace amounts of Sr in magnesium-rich samples. *Journal of Mineralogy, Petrology and Economic Geology*, *88*(12), 548–561. https://doi.org/10.2465/ganko.88.548

Yu, C., Shi, X., Yang, X., Zhao, J., Chen, M., & Tang, Q. (2017). Deep thermal structure of Southeast Asia constrained by S-velocity data. *Marine Geophysical Research*, *38*(4), 341–355. https://doi.org/10.1007/s11001-017-9311-x

Yu, Y., Gao, S. S., Liu, K. H., Yang, T., Xue, M., & Le, K. P. (2017a). Mantle transition zone discontinuities beneath the Indochina Peninsula: Implications for slab subduction and mantle upwelling. *Geophysical Research Letters*, *44*(14), 7159–7167. https://doi.org/10.1002/2017gl073528

Yu, Y., Hung, T. D., Yang, T., Xue, M., Liu, K. H., & Gao, S. S. (2017b). Lateral variations of crustal structure beneath the Indochina Peninsula. *Tectonophysics*, *712–713*, 193–199. https://doi.org/10.1016/j.tecto.2017.05.023

Zhang, G.-L., Chen, L.-H., Jackson, M. G., & Hofmann, A. W. (2017). Evolution of carbonated melt to alkali basalt in the South China Sea. *Nature Geoscience*, *10*(3), 229–235. https://doi.org/10.1038/ngeo2877

Zhang, G.-L., Luo, Q., Zhao, J., Jackson, M. G., Guo, L.-S., & Zhong, L.-F. (2018). Geochemical nature of sub-ridge mantle and opening dynamics of the South China Sea. *Earth and Planetary Science Letters*, *489*, 145–155. https://doi.org/10.1016/j.epsl.2018.02.040

Zhang, G.-L., Sun, W.-D., & Seward, G. (2018b). Mantle source and magmatic evolution of the dying spreading ridge in the South China Sea. *Geochemistry, Geophysics, Geosystems*, *19*(11), 4385–4399. https://doi.org/10.1029/2018GC007570

Zhao, D., Toyokuni, G., & Kurata, K. (2021). Deep mantle structure and origin of Cenozoic intraplate volcanoes in Indochina, Hainan and South China Sea. *Geophysical Journal International*, *225*(1), 572–588. https://doi.org/10.1093/gji/ggaa605

Zhou, P., & Mukasa, S. (1997). Nd-Sr-Pb isotopic, and major- and trace-element geochemistry of Cenozoic: Lavas from the Khorat Plateau, Thailand: Sources and petrogenesis. *Chemical Geology*, *137*, 175–193. https://doi.org/10.1016/S0009-2541(96)00162-3

Zindler, A., & Hart, S. (1986). Chemical Geodynamics. *Annual Review of Earth and Planetary Sciences*, *14*(1), 493–571. https://doi.org/10.1146/annurev.ea.14.050186.002425

References From the Supporting Information

Adam, J., & Green, T. (2006). Trace element partitioning between mica- and amphibole-bearing garnet lherzolite and hydrous basanitic melt: 1. Experimental results and the investigation of controls on partitioning behaviour. *Contributions to Mineralogy and Petrology*, *152*(1), 1–17. https://doi.org/10.1007/s00410-006-0085-4

Bacon, C. R., & Druitt, T. H. (1988). Compositional evolution of the zoned calcalkaline magma chamber of Mount Mazama, Crater Lake, Oregon. *Contributions to Mineralogy and Petrology*, *98*(2), 224–256. https://doi.org/10.1007/BF00402114

Barr, S. M., & Cooper, M. A. (2013). Late Cenozoic basalt and gabbro in the subsurface in the Phetchabun Basin, Thailand: Implications for the Southeast Asian Volcanic Province. *Journal of Asian Earth Sciences*, *76*, 169–184. https://doi.org/10.1016/j.jseaes.2013.01.013

Beattie, P. (1994). Systematics and energetics of trace-element partitioning between olivine and silicate melts: Implications for the nature of mineral/melt partitioning. *Chemical Geology*, *117*(1-4), 57–71. https://doi.org/10.1016/0009-2541(94)90121-X

Cabral, R. A., Jackson, M. G., Koga, K. T., Rose-Koga, E. F., Hauri, E. H., Whitehouse, M. J., et al. (2014). Volatile cycling of H_2O, CO_2, F, and Cl in the HIMU mantle: A new window provided by melt inclusions from oceanic hot spot lavas at Mangaia, Cook Islands. *Geochemistry, Geophysics, Geosystems*, *15*(11), 4445–4467. https://doi.org/10.1002/2014GC005473

Danyushevsky, L. V., Eggins, S. M., Falloon, T. J., & Christie, D. M. (2000). H_2O abundance in depleted to moderately enriched mid-ocean ridge magmas; Part I: Incompatible behaviour, implications for mantle storage, and origin of regional variations. *Journal of Petrology*, *41*(8), 1329–1364. https://doi.org/10.1093/petrology/41.8.1329

Dasgupta, R., Hirschmann, M. M., & Stalker, K. (2006). Immiscible transition from carbonate-rich to silicate-rich melts in the 3 GPa melting interval of eclogite + CO_2 and genesis of silica-undersaturated ocean island lavas. *Journal of Petrology*, *47*(4), 647–671. https://doi.org/10.1093/petrology/egi088

Dasgupta, R., Hirschmann, M. M., & Smith, N. D. (2007). Partial melting experiments of peridotite + CO_2 at 3 GPa and genesis of alkalic ocean island basalts. *Journal of Petrology*, *48*(11), 2093–2124. https://doi.org/10.1093/petrology/egm053

Elkins, L. J., Gaetani, G. A., & Sims, K. W. W. (2008). Partitioning of U and Th during garnet pyroxenite partial melting: Constraints on the source of alkaline ocean island basalts. *Earth and Planetary Science Letters*, *265*(1), 270–286. https://doi.org/10.1016/j.epsl.2007.10.034

Foley, S. F., Prelevic, D., Rehfeldt, T., & Jacob, D. E. (2013). Minor and trace elements in olivines as probes into early igneous and mantle melting processes. *Earth and Planetary Science Letters*, *363*, 181–191. https://doi.org/10.1016/j.epsl.2012.11.025

Hauff, F., Hoernle, K., & Schmidt, A. (2003). Sr-Nd-Pb composition of Mesozoic Pacific oceanic crust (Site 1149 and 801, ODP Leg 185): Implications for alteration of ocean crust and the input into the Izu-Bonin-Mariana subduction system. *Geochemistry, Geophysics, Geosystems*, *4*(8), 8913. https://doi.org/10.1029/2002GC000421

Hirschmann, M. M. (2018). Comparative deep Earth volatile cycles: The case for C recycling from exosphere/mantle fractionation of major (H_2O, C, N) volatiles and from H_2O/Ce, CO_2/Ba, and CO_2/Nb exosphere ratios. *Earth and Planetary Science Letters*, *502*, 262–273. https://doi.org/10.1016/j.epsl.2018.08.023

Keshav, S., Gudfinnsson, G. H., Sen, G., & Fei, Y. (2004). High-pressure melting experiments on garnet clinopyroxenite and the alkalic to tholeiitic transition in ocean-island basalts. *Earth and Planetary Science Letters*, *223*(3), 365–379. https://doi.org/10.1016/j.epsl.2004.04.029

Klemme, S., Günther, D., Hametner, K., Prowatke, S., & Zack, T. (2006). The partitioning of trace elements between ilmenite, ulvospinel, armalcolite and silicate melts with implications for the early differentiation of the moon. *Chemical Geology*, *234*(3), 251–263. https://doi.org/10.1016/j.chemgeo.2006.05.005

Krolikowska-Ciaglo, S., Hauff, F., & Hoernle, K. (2005). Sr-Nd isotope systematics in 14–28 Ma low-temperature altered mid-ocean ridge basalt from the Australian Antarctic Discordance, Ocean Drilling Program Leg 187. *Geochemistry, Geophysics, Geosystems*, *6*(1), Q01001. https://doi.org/10.1029/2004GC000802

Kuritani, T., & Nakamura, E. (2002). Precise isotope analysis of nanogram-level Pb for natural rock samples without use of double spikes. *Chemical Geology*, *186*(1), 31–43. https://doi.org/10.1016/S0009-2541(02)00004-9

Kuritani, T., & Nakamura, E. (2003). Highly precise and accurate isotopic analysis of small amounts of Pb using ^{205}Pb-^{204}Pb and ^{207}Pb-^{204}Pb, two double spikes. *Journal of Analytical Atomic Spectrometry*, *18*(12), 1464–1470. https://doi.org/10.1039/B310294G

Lambart, S., Laporte, D., Provost, A., & Schiano, P. (2012). Fate of pyroxenite-derived melts in the peridotitic mantle: Thermodynamic and experimental constraints. *Journal of Petrology*, *53*(3), 451–476. https://doi.org/10.1093/petrology/egr068

Lambart, S., Laporte, D., & Schiano, P. (2009a). An experimental study of focused magma transport and basalt–peridotite interactions beneath mid-ocean ridges: Implications for the generation of primitive MORB compositions. *Contributions to Mineralogy and Petrology*, *157*(4), 429–451. https://doi.org/10.1007/s00410-008-0344-7

Lambart, S., Laporte, D., & Schiano, P. (2009b). An experimental study of pyroxenite partial melts at 1 and 1.5 GPa: Implications for the major-element composition of Mid-Ocean Ridge Basalts. *Earth and Planetary Science Letters*, *288*(1), 335–347. https://doi.org/10.1016/j.epsl.2009.09.038

Lambart, S., Laporte, D., & Schiano, P. (2013). Markers of the pyroxenite contribution in the major-element compositions of oceanic basalts: Review of the experimental constraints. *Lithos*, *160–161*, 14–36. https://doi.org/10.1016/j.lithos.2012.11.018

Lepvrier, C., Maluski, H., Van Tich, V., Leyreloup, A., Thi, P. T., & Van Vuong, N. (2004). The early Triassic Indosinian orogeny in Vietnam (Truong Son Belt and Kontum Massif); implications for the geodynamic evolution of Indochina. *Tectonophysics*, *393*(1-4), 87–118. https://doi.org/10.1016/j.tecto.2004.07.030

Lu, Y., Makishima, A., & Nakamura, E. (2007). Coprecipitation of Ti, Mo, Sn and Sb with fluorides and application to determination of B, Ti, Zr, Nb, Mo, Sn, Sb, Hf and Ta by ICP-MS. *Chemical Geology*, *236*(1), 13–26. https://doi.org/10.1016/j.chemgeo.2006.08.007

Makishima, A., Nath, B. N., & Nakamura, E. (2008). New sequential separation procedure for Sr, Nd and Pb isotope ratio measurement in geological material using MC-ICP-MS and TIMS. *Geochemical Journal*, *42*(3), 237–246. https://doi.org/10.2343/geochemj.42.237

Maluski, H., Lepvrier, C., Leyreloup, A., Van Tich, V., & Thi, P. T. (2005). ^{40}Ar–^{39}Ar geochronology of the charnockites and granulites of the Kan Nack complex, Kon Tum Massif, Vietnam. *Journal of Asian Earth Sciences*, *25*(4), 653–677. https://doi.org/10.1016/j.jseaes.2004.07.004

McKenzie, D. A. N., & O'Nions, R. K. (1991). Partial melt distributions from inversion of rare earth element concentrations. *Journal of Petrology*, *32*(5), 1021–1091. https://doi.org/10.1093/petrology/32.5.1021

Michael, P. (1995). Regionally distinctive sources of depleted MORB: Evidence from trace elements and H_2O. *Earth and Planetary Science Letters*, *131*(3), 301–320. https://doi.org/10.1016/0012-821X(95)00023-6

Nagao, K., Ogata, A., Miura, Y. N., & Yamaguchi, K. (1996). Ar isotope analysis for K-Ar dating using two modified-VG5400 mass spectrometers—I: Isotope dilution method. *Journal of the Mass Spectrometry Society of Japan*, *44*(1), 39–61. https://doi.org/10.5702/massspec.44.39

Nguyen, H. H., Pham, N. S., Hoang, V. L., Andrew, C., Bui, V. H., Bui, H. B., et al. (2021). Cretaceous granitic magmatism in South-Central Vietnam: Constraints from zircon U–Pb geochronology. *Journal of the Polish Mineral Engineering Society*, *1*(2), 7–14. https://doi.org/10.29227/IM-2021-02-01

Nier, A. O. (1950). A redetermination of the relative abundances of the isotopes of carbon, nitrogen, oxygen, argon, and potassium. *Physical Review*, *77*(6), 789–793. https://doi.org/10.1103/PhysRev.77.789

Patte, É. (1925). Étude de l'île des Cendres, volcan apparu au large de la côte d'Annam, par Étienne Patte. Impr. d'Extrême-Orient. *Bulletin du Service G ´eologique de l'Indochine*, *13*, 1–19.

Pilet, S., Baker, M. B., Müntener, O., & Stolper, E. M. (2011). Monte Carlo simulations of metasomatic enrichment in the lithosphere and implications for the source of alkaline basalts. *Journal of Petrology*, *52*(7–8), 1415–1442. https://doi.org/10.1093/petrology/egr007

Ronov, A. B., & Yaroshevskiy, A. A. (1976). A new model for the chemical structure of the Earth's crust. *Geochemistry International*, *13*(6), 89–121.

Shellnutt, J. G., Lan, C. Y., Van Long, T., Usuki, T., Yang, H. J., Mertzman, S. A., et al. (2013). Formation of Cretaceous Cordilleran and post-orogenic granites and their microgranular enclaves from the Dalat zone, southern Vietnam: Tectonic implications for the evolution of Southeast Asia. *Lithos*, *182-183*, 229–241. https://doi.org/10.1016/j.lithos.2013.09.016

Steiger, R. H., & Jäger, E. (1977). Subcommission on geochronology: Convention on the use of decay constants in geo- and cosmochronology. *Earth and Planetary Science Letters*, *36*(3), 359–362. https://doi.org/10.1016/0012-821X(77)90060-7

Stracke, A., Hofmann, A. W., & Hart, S. R. (2005). FOZO, HIMU, and the rest of the mantle zoo. *Geochemistry, Geophysics, Geosystems*, *6*(5). https://doi.org/10.1029/2004GC000824

Takei, H. (2002). *Development of precise analytical techniques for major and trace element concentrations in rock samples and their applications to the Hishikari Gold Mine, southern Kyushu, Japan (Ph. D Thesis)*, Okayama University,

Tran, T. H., Lan, C. Y., Usuki, T., Shellnutt, J. G., Pham, T. D., Tran, T. A., et al. (2015). Petrogenesis of Late Permian silicic rocks of Tu Le basin and Phan Si Pan uplift (NW Vietnam) and their association with the Emeishan large igneous province. *Journal of Asian Earth Sciences*, *109*, 1–19. https://doi.org/10.1016/j.jseaes.2015.05.009

Yaxley, G. M., & Green, D. H. (1998). Reactions between eclogite and peridotite: Mantle refertilisation by subduction of oceanic crust. *Schweizerische Mineralogische und Petrographische Mitteilungen*, *78*(2), 243–255.